Mammalian spontaneous otoacoustic emissions are amplitude-stabilized cochlear standing waves

Christopher A. Shera[a)]
Eaton-Peabody Laboratory of Auditory Physiology, Massachusetts Eye and Ear Infirmary, 243 Charles Street, Boston, Massachusetts 02114 and Department of Otology and Laryngology, Harvard Medical School, Boston, Massachusetts 02115

(Received 11 December 2002; revised 20 March 2003; accepted 24 March 2003)

Mammalian spontaneous otoacoustic emissions (SOAEs) have been suggested to arise by three different mechanisms. The local-oscillator model, dating back to the work of Thomas Gold, supposes that SOAEs arise through the local, autonomous oscillation of some cellular constituent of the organ of Corti (e.g., the ''active process'' underlying the cochlear amplifier). Two other models, by contrast, both suppose that SOAEs are a global collective phenomenon—cochlear standing waves created by multiple internal reflection—but differ on the nature of the proposed power source: Whereas the ''passive'' standing-wave model supposes that SOAEs are biological noise, passively amplified by cochlear standing-wave resonances acting as narrow-band nonlinear filters, the ''active'' standing-wave model supposes that standing-wave amplitudes are actively maintained by coherent wave amplification within the cochlea. Quantitative tests of key predictions that distinguish the local-oscillator and global standing-wave models are presented and shown to support the global standing-wave model. In addition to predicting the existence of multiple emissions with a characteristic minimum frequency spacing, the global standing-wave model accurately predicts the mean value of this spacing, its standard deviation, and its power-law dependence on SOAE frequency. Furthermore, the global standing-wave model accounts for the magnitude, sign, and frequency dependence of changes in SOAE frequency that result from modulations in middle-ear stiffness. Although some of these SOAE characteristics may be replicable through artful *ad hoc* adjustment of local-oscillator models, they all arise quite naturally in the standing-wave framework. Finally, the statistics of SOAE time waveforms demonstrate that SOAEs are coherent, amplitude-stabilized signals, as predicted by the active standing-wave model. Taken together, the results imply that SOAEs are amplitude-stabilized standing waves produced by the cochlea acting as a biological, hydromechanical analog of a laser oscillator. Contrary to recent claims, spontaneous emission of sound from the ear does not require the autonomous mechanical oscillation of its cellular constituents. [DOI: 10.1121/1.1575750]

PACS numbers: 43.64.Bt, 43.64.Kc, 43.64.Jb, 43.64.Ha, 43.25.Gf [BLM]

I. INTRODUCTION

Spontaneous otoacoustic emissions (SOAEs), first reported in 1979 (Kemp, 1979a; Wilson, 1980; Zurek, 1981), are commonly thought to arise through a mechanism whose essentials were described some 30 years earlier (Gold, 1948). Discussing the implications of his ''regeneration hypothesis'' that electromechanical feedback somehow counteracts the viscous damping in the cochlea, Gold noted that ''if the feedback ever exceeded the losses, then a resonant element [in the organ of Corti] would become self-oscillatory, and oscillations would build up [to] a level where linearity was not preserved.'' Despite the ''self-regulating mechanism,'' whose existence he postulated as necessary to control the amount of feedback, Gold suggested that

> ''We might expect that occasional disturbances would bring an element into the region of self-oscillation, when it is normally so close to this condition. If this occurred, then we should hear a clear note which would persist until the adjusting mechanism has regained control, or until the nervous sensitivity has decreased sufficiently.''

Fifty years after Gold's prediction, the vocabulary is new but the basic idea remains unchanged:

> ''Such a self-tuning mechanism provides a natural explanation for spontaneous emissions of sound from the ear. Normally, the low-amplitude vibration of the self-tuned critical oscillators would produce a faint hum. But if one of the motile systems were to have a faulty control mechanism, it might oscillate wildly, generating a shrill whistle.'' (Duke, 2002).

The descriptions quoted here share with many others in the literature a key feature: They identify the ''oscillating element'' responsible for spontaneous emission of sound as *local* to a particular place along the cochlea. Often the putative oscillating element is localized even further within a cochlear cross section and identified with ''certain cells'' or parts of cells (e.g., hair-cell stereocilia) within the organ of Corti. Martin and Hudspeth (2001), for example, adopt this view when arguing that ''unprovoked movements of some

a)Electronic mail: shera@epl.meei.harvard.edu

constituent of the ear's amplifier are expected to underlie the production of spontaneous otoacoustic emissions.''

A. Local oscillator or global standing-wave resonance?

Despite wide acceptance of the local-oscillator model of SOAEs, there exists another possibility for SOAE generation, a possibility first suggested by Kemp (1979a, 1979b) and subsequently elaborated in models of evoked otoacoustic emissions (e.g., Zwicker and Peisl, 1990; Zweig, 1991; Talmadge and Tubis, 1993; Zweig and Shera, 1995; Allen *et al.*, 1995; Talmadge *et al.*, 1998; Shera and Guinan, 1999). These models of evoked emissions predict that mammalian SOAEs arise not via autonomous cellular oscillations but as cochlear standing-wave resonances. In this view, SOAEs result from multiple internal reflection of traveling-wave energy initiated either by sounds from the environment or by physiological noise.

The theory of reflection-source emissions (Shera and Zweig, 1993b; Zweig and Shera, 1995; Talmadge *et al.*, 1998), for example, predicts that backward-traveling cochlear waves are generated by the coherent scattering of forward-traveling waves off densely and randomly distributed perturbations in the mechanics of the cochlea. Because wavelets scattered near the peak of a forward-traveling wave have much larger amplitudes than those reflected elsewhere, the net reflected wave is dominated by scattering that occurs in the region about the response maximum. The resulting backward-traveling waves are then reflected by the impedance mismatch at the cochlear boundary with the middle ear, generating additional forward-traveling waves that subsequently undergo another round of coherent reflection near their characteristic places. At frequencies for which the total phase change due to round-trip wave travel is an integral number of cycles, standing waves can build up within the cochlea, which is then acting, in effect, as a tuned resonant cavity. Cochlear standing waves can become self-sustaining—and thus appear in the ear canal as spontaneous emissions—when the total round-trip power gain matches the energy losses (e.g., from viscous damping and acoustic radiation into the ear canal) experienced en route.

The standing-wave model differs fundamentally from the local-oscillator scenario. Rather than supposing that the ''oscillating elements'' generating SOAEs are localized to particular cells or subcellular structures within the organ of Corti, the standing-wave model identifies SOAEs as a *global collective phenomenon* necessarily involving the mechanics, hydrodynamics, and cellular physiology of the entire cochlea, as well as the mechanical and acoustical loads presented to it by the middle and external ears. In the local-oscillator model these macromechanical structures and processes play no fundamental role—they serve merely to connect the autonomous oscillating element with the external environment, providing a conduit for the acoustic energy it produces to escape from the inner ear. In the global standing-wave model, by contrast, the oscillating element comprises the entire cochlea, and the collective response of the hearing organ as a whole contributes essentially to creating, maintaining, and determining the characteristics of the emission.

B. Overview

This paper tests these two alternative models for the origin of mammalian SOAEs. Our discussion focuses on key predictions of the global standing-wave model that distinguish it from the local-oscillator alternative. Although some of these predictions could perhaps be obtained by artful adjustment of local-oscillator models, they all arise quite naturally within the standing-wave framework without the need for additional *ad hoc* assumptions. We therefore begin with a brief review of the global standing-wave model and its distinguishing predictions. In particular, we use the model to derive quantitative answers to questions such as ''What is so special about SOAE frequencies? Why do the SOAEs observed in a particular ear occur at *these* frequencies and not others? and What determines the distribution of SOAE frequency spacings?''[1] Many of the resulting model predictions, which generally involve correlations between spontaneous and evoked emissions and/or the modulation of SOAEs by changes in middle-ear impedance, have been explored in various ways elsewhere (e.g., Kemp, 1979b; Wilson, 1980; Zwicker and Schloth, 1984; Zweig and Shera, 1995; Allen *et al.*, 1995; Talmadge *et al.*, 1998). We extend this earlier work by providing quantitative tests of standing-wave model predictions at frequencies spanning the entire range over which human SOAEs have been reported. Our results provide strong support for the global standing-wave model.

We continue by testing the predictions of two very different versions of the global standing-wave model appearing in the literature. These two alternative standing-wave models differ in the nature of the proposed power source. Whereas the ''passive'' standing-wave model supposes that SOAEs are biological noise, passively amplified by cochlear standing-wave resonances acting as narrow-band nonlinear filters (Allen and Fahey, 1992; Allen *et al.*, 1995; Allen, 2001), the ''active'' standing-wave model supposes that standing-wave amplitudes are actively maintained by coherent wave amplification within the cochlea (Kemp, 1979a; Zweig, 1991; Talmadge and Tubis, 1993; Zweig and Shera, 1995; Talmadge *et al.*, 1998). Our test contributes to the literature on the differences between passive and active SOAE sources (e.g., Bialek and Wit, 1984; Talmadge *et al.*, 1991; Allen *et al.*, 1995; Tubis and Talmadge, 1998; Burns *et al.*, 1998) by providing a compelling empirical demonstration of the special character of SOAEs—amplitude stabilization—that distinguishes them from narrow-band filtered noise. Taken together, our results strongly support the active standing-wave model, which suggests that SOAEs are coherent, amplitude-stabilized acoustic signals produced by the cochlea acting as a biological, hydromechanical analog of a laser oscillator.

II. THE GLOBAL STANDING-WAVE MODEL OF SOAEs

The global standing-wave model of SOAEs posits a close connection between spontaneous otoacoustic emissions and a particular type of evoked emission, namely stimulus-frequency OAEs (or SFOAEs), which are sounds evoked from the ear at the frequency of the stimulus. In a nutshell, the global standing-wave model suggests that SOAEs are

continuously self-evoking stimulus-frequency emissions initiated either by sounds from the environment or by thermal or physiological noise internal to the cochlea.

To deduce characteristics of SOAEs we begin by considering the SFOAE evoked by a low-level pure tone. We interpret the SFOAE as indicating the presence of a backward-traveling wave within the cochlea. To characterize this wave we define the cochlear traveling-wave reflectance, R, as the complex ratio of the out-going (backward-traveling) to the in-going (forward-traveling) pressure wave at the basal end of the cochlea near the stapes (Shera and Zweig, 1993a; Zweig and Shera, 1995; Talmadge *et al.*, 1998):

$$R(f;P_{\text{in}}) \equiv \left. \frac{P_{\text{out}}(f;P_{\text{in}})}{P_{\text{in}}(f)} \right|_{\text{stapes}}. \tag{1}$$

We define $R(f;P_{\text{in}})$ as the reflectance measured at the stapes—rather than introduce a local reflection coefficient (R_x) for every point x within the cochlea (e.g., Kemp, 1979b; Allen, 2001)—because no simple relation between R_x and the total backward-traveling wave exists when wave scattering occurs over a distributed region (Zweig and Shera, 1995).[2] The cochlear reflectance $R(f;P_{\text{in}})$ depends on both the frequency, f, and on the amplitude of the in-going pressure wave, P_{in}. At sound levels in the low-level linear regime near threshold, P_{out} is proportional to P_{in} and R is therefore independent of level (Shera and Zweig, 1993a); at higher sound levels, the amplitude of P_{out} is compressed relative to P_{in} and $|R(f;P_{\text{in}})|$ decreases towards zero. The function $R(f;P_{\text{in}})$ provides a phenomenological characterization of the emission process as seen from the base of the cochlea; according to the coherent-reflection model, its value at any given frequency depends both on the distribution of reflecting impedance perturbations and on the magnitude of round-trip traveling-wave amplitude gains or losses.

By regarding the intervening ear-canal space and middle ear as a linear acousto-mechanical two-port system (Egolf *et al.*, 1992; Peake *et al.*, 1992; Shera and Zweig, 1992b; Puria, 2003) characterized in the frequency domain using reflectance and transmittance coefficients (Shera and Zweig, 1992a; Keefe *et al.*, 1993; Voss and Allen, 1994), one can relate the stimulus-frequency emission measured in the ear canal (P_{SFOAE}) to the value of the cochlear reflectance:

$$P_{\text{SFOAE}} = P_0 G_{\text{mert}} \frac{R(1+R_{\text{stapes}})}{1-RR_{\text{stapes}}}, \tag{2}$$

where $P_0(f)$ is the stimulus source pressure,[3] $G_{\text{mert}}(f)$ is the round-trip middle-ear pressure transfer function,[4] and $R_{\text{stapes}}(f)$ is the reflection coefficient for retrograde cochlear waves at the stapes (Shera and Zweig, 1991a; Zweig and Shera, 1995; Talmadge *et al.*, 1998).[5] The value of R_{stapes} depends not only on the mechanics of the middle ear but also on the acoustic load present in the ear canal (e.g., the ear-canal radiation impedance or the equivalent acoustic impedance of any measurement system placed in the meatus).[6] Note that the values of G_{mert} and R_{stapes} are not independent; energy conservation implies that $|G_{\text{mert}}| \to 0$ as $|R_{\text{stapes}}| \to 1$.

A. Standing waves from multiple internal reflection

The factor $R/(1-RR_{\text{stapes}})$ in Eq. (2) arises from multiple internal reflection within the cochlea, a phenomenon well documented in both the time and frequency domains (e.g., Norton and Neely, 1987; Shera and Zweig, 1993a; Konard-Martin *et al.*, 2001; Dhar *et al.*, 2002). To see this, note that for $|RR_{\text{stapes}}|<1$ the factor is simply the sum of the infinite series

$$R[1+RR_{\text{stapes}}+(RR_{\text{stapes}})^2+\cdots] = R\sum_{n=0}^{\infty}(RR_{\text{stapes}})^n. \tag{3}$$

The terms in this power series can be understood physically as follows. Suppose that the initial forward-traveling wave has unit amplitude at the stapes ($P_{\text{in}}=1$). This primary forward-traveling wave propagates down the cochlear spiral and is partially reflected (re-emitted) in more apical regions of the cochlea. When it returns to the stapes the resulting backward-traveling wave has an amplitude, R, given by the first ($n=0$) term in the power series [see Eq. (1) with $P_{\text{in}}=1$]. At the stapes, the backward wave of amplitude R is then partially reflected back into the cochlea, creating a secondary forward-traveling wave of amplitude RR_{stapes}. This secondary forward-traveling wave is in turn reflected/re-emitted within the cochlea, creating then a secondary backward-traveling wave whose amplitude at the stapes, R^2R_{stapes}, is given by the second ($n=1$) term in the series. The process of multiple reflection continues, each subsequent stapes reflection and cochlear re-emission contributing an additional backward-traveling wave whose amplitude at the stapes differs by a factor of RR_{stapes} from the one before. Adding up all the backward-traveling waves (i.e., summing the power series) yields the factor $R/(1-RR_{\text{stapes}})$ in Eq. (2) for P_{SFOAE}.

Whenever the product RR_{stapes} is positive real, the secondary, tertiary, and all higher-order forward-traveling waves combine in phase with the primary traveling wave at the stapes. The multiple internal reflections then reinforce one another, creating a significant standing-wave component in the cochlear response whose amplitude depends on the product of cochlear and stapes reflection factors, RR_{stapes}. Equation (2) predicts that the standing wave grows without bound as RR_{stapes} approaches 1.[7] In the real cochlea, of course, unconstrained growth is prevented by compressive nonlinearities that limit the energy produced. Once initiated—whether by sounds from the environment or by physiological noise—standing waves of this sort require no external sound for their maintenance;[8] they would be manifest in the ear canal as spontaneous otoacoustic emissions. The standing-wave model thus emphasizes the global nature of SOAEs, with a key role played by the impedance mismatch at the cochlear boundary with the middle ear. Indeed, standing-wave SOAEs would never arise if the stapes and adjoining structures combined to present a perfectly reflectionless boundary ($R_{\text{stapes}} \to 0$).

III. TESTING THE GLOBAL STANDING-WAVE MODEL

Whenever the round-trip amplitude (or standing-wave) gain is sufficient to maintain the emission [i.e., $|RR_{\text{stapes}}|$

$=1$ in the linear analysis of Eq. (2)], the global standing-wave model predicts that SOAEs occur at frequencies f_{SOAE} where RR_{stapes} is positive real. If $\theta(f)$ represents the angle of RR_{stapes}, so that

$$\theta(f) \equiv \angle\{RR_{\mathrm{stapes}}\}, \tag{4}$$

then SOAE frequencies f_{SOAE} satisfy the equation

$$\theta(f_{\mathrm{SOAE}}) = 2\pi n, \tag{5}$$

for some integral value of n. Although neither R nor R_{stapes} is directly accessible noninvasively, a number of indirect tests of the model can be made by using SFOAEs to determine the frequency dependence of $\theta(f)$.

A. The frequency dependence of $\theta(f)$

We obtain the principal frequency dependence of $\theta(f)$ by writing it in the form

$$\theta(f) = \angle R(f) + \angle R_{\mathrm{stapes}}(f), \tag{6}$$

and exploiting two well-established characteristics of SFOAEs at low sound levels.

(1) First, although relative SFOAE amplitudes (i.e., $|P_{\mathrm{SFOAE}}/P_0|$) decrease rapidly with increasing sound intensity, SFOAE phase varies much less strongly with level (e.g., Kemp and Chum, 1980; Zwicker and Schloth, 1984; Shera and Zweig, 1993a). We can therefore estimate $\angle R$ at the relatively low sound levels typical of SOAEs (where $|R|$ is of order 1) using measurements of P_{SFOAE} made at higher levels (where $|R| \ll 1$). [We later correct for the small systematic error introduced by this approximation (see Sec. V A).] When $|R|$ is small Eq. (2) reduces to

$$P_{\mathrm{SFOAE}} \approx P_0 G_{\mathrm{mert}} R(1 + R_{\mathrm{stapes}}) \quad (|R| \ll 1). \tag{7}$$

Solving this equation for R and using the result in Eq. (6) yields

$$\theta(f) \approx \angle P_{\mathrm{SFOAE}} + \angle\{R_{\mathrm{stapes}}/G_{\mathrm{mert}}(1 + R_{\mathrm{stapes}})\}, \tag{8}$$

where $\angle P_0$ has been defined to be zero.

(2) Second, SFOAE phase varies much more rapidly with frequency than do the phases of middle-ear transfer functions. Figure 1 shows a polar plot of typical measurements of $P_{\mathrm{SFOAE}}(f)$ in humans. Although $|P_{\mathrm{SFOAE}}|$ generally varies relatively slowly with frequency, $\angle P_{\mathrm{SFOAE}}(f)$ rotates rapidly, encircling the origin more than 8 times over the frequency range of the data (roughly 1–2 kHz). Since the "angular velocity" (or phase slope) of the rotation is large and nearly constant over intervals comparable to several orbital periods, SFOAE phase changes almost uniformly with frequency. At these frequencies the average orbital period is about 125 Hz; over the frequency range 1–10 kHz, $\angle P_{\mathrm{SFOAE}}(f)$ circles the origin roughly 40 times, yielding an average period of about 225 Hz (Shera and Guinan, 2003). The phases of middle-ear transfer functions, by contrast, vary much more slowly (e.g., Puria *et al.*, 1997; Puria, 2003). Computing $R_{\mathrm{stapes}}/G_{\mathrm{mert}}(1 + R_{\mathrm{stapes}})$ using Puria's (2003) measurements in human cadavers indicates that the middle-ear component of $\theta(f)$ [i.e., the second term in Eq. (8)] amounts to only a single cycle from 1–10 kHz. The middle-ear thus contributes an average phase slope some 40 times smaller than that of P_{SFOAE}.

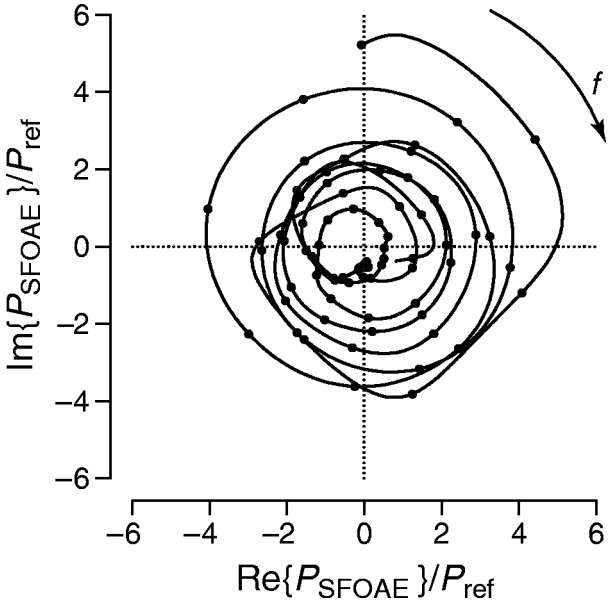

FIG. 1. Polar plot of typical human SFOAEs. The measurements (●) of $P_{\mathrm{SFOAE}}(f)$ were obtained using a variant of the suppression method (Shera and Guinan, 1999) at a stimulus level of 40 dB SPL (subject MAB-L). The axes give the real and imaginary parts of $P_{\mathrm{SFOAE}}/P_{\mathrm{ref}}$, where P_{ref} is 20 μPa. The measurement noise floor is approximately 0.05 in these units. The smooth solid line connecting the data points was computed using bandlimited interpolation. The figure shows $P_{\mathrm{SFOAE}}(f)$ circling clockwise about the origin as frequency increases; the phase traverses more than 8 cycles over the frequency range of the data (0.9–1.9 kHz). Figure 9 of Shera and Guinan (1999) shows these same data in an alternate form (amplitude and phase versus frequency).

Combining items (1) and (2) above, we conclude that as approximated by Eq. (8) the overall frequency dependence of $\theta(f)$ is dominated by $\angle P_{\mathrm{SFOAE}}(f)$. To a good first approximation, Eq. (8) becomes

$$\theta(f) \approx \angle P_{\mathrm{SFOAE}}(f) + \text{constant}, \tag{9}$$

meaning that relative to $\angle P_{\mathrm{SFOAE}}$ the second, "constant" term in Eq. (8) changes slowly with f, at least in humans. We can therefore test the global standing-wave model noninvasively using stimulus-frequency otoacoustic emissions.

IV. QUALITATIVE PREDICTIONS OF THE MODEL

Since $\theta(f)$ evidently rotates through many cycles over the frequency range of human hearing (see Fig. 1), the global standing-wave model predicts that multiple solutions to Eq. (5), and therefore multiple SOAEs, are possible in a single ear. Multiple SOAEs are, in fact, commonly observed experimentally. The study by Talmadge *et al.* (1993) found that roughly 80% of all emitting ears had more than one SOAE (with a median of 5 SOAEs per emitting ear). Since $\theta(f)$

changes (nearly) monotonically, multiple SOAEs can be indexed by the value of n in Eq. (5) and their frequencies written $f_{\mathrm{SOAE}}^{(n)}$.

In the global standing-wave model, the observation that $\theta(f)$ rotates almost uniformly imposes an approximate quantization on the frequency spacing between multiple emissions. The standing-wave quantization condition, namely[9]

$$\theta(f_{\mathrm{SOAE}}^{(n)}) = 2\pi n \quad (n = 0, \pm 1, \ldots), \tag{10}$$

follows from the requirement that forward-traveling waves reflected from the stapes combine in phase with one another. Equation (10) implies that if the round-trip amplitude gain were everywhere sufficient, the spacing between adjacent emissions, Δf_{SOAE}, would be equal to the interval, Δf_{θ}, over which $\theta(f)$ changes by one cycle:

$$\Delta f_{\mathrm{SOAE}}(f) = \Delta f_{\theta}(f). \tag{11}$$

If $\theta(f)$ were to rotate at a constant rate, multiple SOAEs would appear with perfectly regular spacing. But, because the rotation rate of $\theta(f)$ varies on frequency scales both large and small, actual emission spacings never manifest such crystalline regularity. Deviations from a constant rotation rate due to the secular phase curvature of $\theta(f)$ become significant over frequency intervals larger than several orbital periods; as a result, the intervals $\Delta f_{\theta}(f)$ and $\Delta f_{\mathrm{SOAE}}(f)$ vary systematically with f. Over smaller frequency intervals, local variability in $\Delta f_{\theta}(f)$ introduces a more stochastic component to SOAE spacings. In addition to the variability in SOAE spacing arising from $\theta(f)$, spatial fluctuations in the round-trip amplitude gain (i.e., the value of $|RR_{\mathrm{stapes}}|$) produce frequent ''drop-outs'' so that most ears manifest only a handful of the potential SOAEs enumerated by Eq. (10).

Despite these sources of variability, the angle $\theta(f)$ does vary almost uniformly over frequency intervals corresponding to several orbital periods. Locally, $\Delta f_{\theta}(f)$ therefore has a well-defined mean, $\overline{\Delta f}_{\theta}(f)$, whose value depends on frequency. The global standing-wave model then predicts that multiple SOAEs will appear with a corresponding characteristic minimum frequency separation, $\overline{\Delta f}_{\mathrm{SOAE}}(f) = \overline{\Delta f}_{\theta}(f)$, corresponding to $|\Delta n| = 1$. Illustrated in Fig. 2 using a histogram of interemission spacings computed from emission data in the literature (Talmadge *et al.*, 1993; Burns *et al.*, 1992), the existence of a characteristic minimum spacing for SOAEs is well documented (e.g., Schloth, 1983; Dalmayr, 1985; Zwicker, 1988; Russell, 1992; Talmadge *et al.*, 1993). Note that the figure represents SOAE spacings in the fractional form $N_{\mathrm{SOAE}} \equiv \overline{f}_{\mathrm{SOAE}}/\Delta f_{\mathrm{SOAE}}$, where $\overline{f}_{\mathrm{SOAE}}$ is the geometric mean frequency of the two SOAEs. The peak at $N_{\mathrm{SOAE}} \approx 15$ corresponds to a characteristic minimum spacing $\overline{\Delta f}_{\mathrm{SOAE}}$ of approximately 100 Hz for SOAEs near 1500 Hz.

We characterize SOAE spacings using the dimensionless representation N_{SOAE} because previous reports suggest that the characteristic spacing $\overline{\Delta f}_{\mathrm{SOAE}}(f)$ increases in direct proportion to emission frequency, with its value corresponding to a constant fraction of an octave [or to what is essentially the same thing, a constant distance along the basilar membrane or a constant fraction of the psychophysical critical band measured in Barks (e.g., Zwicker, 1989; Talmadge *et al.*, 1993; Braun, 1997)]. It is therefore conventional to express the interval $\overline{\Delta f}_{\mathrm{SOAE}}(f)$ in some relative form (e.g., as a fraction of an octave) rather than directly in Hz. We later demonstrate the systematic deviations from these conventional representations predicted by the global standing-wave model (see Secs. V A and VII E).

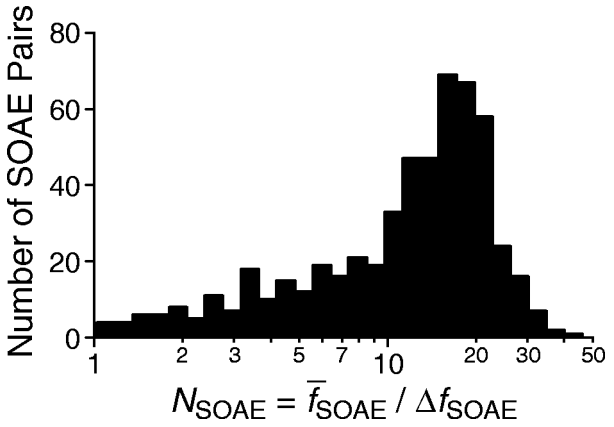

FIG. 2. Histogram of human SOAE spacings. The figure shows a histogram of values of N_{SOAE}, defined as $\overline{f}_{\mathrm{SOAE}}/\Delta f_{\mathrm{SOAE}}$, computed from adjacent pairs of SOAEs reported in compilations of adult (Talmadge *et al.*, 1993) and child (Burns *et al.*, 1992) SOAE data. The spacing Δf_{SOAE} is the absolute value of the difference between the two SOAE frequencies; $\overline{f}_{\mathrm{SOAE}}$ is their geometric mean. The adult data represent 503 SOAE pairs from 67 ears in 44 subjects (age 7–49 years); the child data represent 53 SOAE pairs from 3 children (age 2). Constant values of N_{SOAE} correspond to constant fractions of an octave, where the fraction, r, is given by $r = \log_2(1 + 1/N_{\mathrm{SOAE}})$. For values $N_{\mathrm{SOAE}} \gg 1$, this simplifies to $1/r \approx \ln 2 \cdot N_{\mathrm{SOAE}}$. For $N_{\mathrm{SOAE}} \approx 15$, the spacing is approximately $\frac{1}{10}$ of an octave.

Figure 2 further demonstrates that $\overline{\Delta f}_{\mathrm{SOAE}}$, the characteristic minimum spacing, also represents the most *common* emission spacing. This result can be understood using the global standing-wave model and the fact that the magnitude of RR_{stapes} changes relatively slowly with frequency compared to its angle, $\theta(f)$. As discussed above, both middle-ear reflectances and SFOAE amplitudes typically vary on frequency scales at least several times larger than $\overline{\Delta f}_{\mathrm{SOAE}}$. Thus, if the round-trip amplitude gain is sufficient to stabilize a standing wave at frequency $f_{\mathrm{SOAE}}^{(n)}$, chances are good that the gain will also suffice at the nearby frequencies $f_{\mathrm{SOAE}}^{(n \pm 1)}$.

In the global standing-wave model, SOAE frequencies are determined in part by the impedance mismatch at the cochlear boundary with the middle ear [see Eq. (5)]. Manipulations that modify this basal boundary condition can therefore modulate both SOAE amplitude (by changing $|R_{\mathrm{stapes}}|$ and/or reverse middle-ear transmission) and, more tellingly, SOAE frequency (by changing $\angle R_{\mathrm{stapes}}$). In accord with these predictions, middle-ear impedance changes—as induced, for example, by varying static ear-canal pressure to tension the tympanic membrane or by modifying the impedance of the annular ligament via postural changes that affect static intracochlear fluid pressure—have been found to alter SOAE characteristics, including frequency (e.g., Kemp, 1981; Wilson and Sutton, 1981; Zurek, 1981; Schloth

and Zwicker, 1983; Bell, 1992; Burns *et al.*, 1993; Hauser *et al.*, 1993; de Kleine *et al.*, 2000).

V. QUANTITATIVE PREDICTIONS OF THE MODEL

We can perform more quantitative tests of the global standing-wave model by expressing the quantization condition in the form

$$\left|\frac{d\theta}{df}\right|\Delta f_\theta \approx 2\pi, \tag{12}$$

where we have approximated the phase slope as constant over the interval Δf_θ, consistent with nearly uniform rotation. Using the observation that the frequency dependence of $\theta(f)$ is dominated by $\angle P_{\mathrm{SFOAE}}$ [Eq. (9)], we obtain the estimate

$$\frac{d\theta}{df} \approx \frac{d\angle P_{\mathrm{SFOAE}}}{df} = -2\pi\tau_{\mathrm{SFOAE}}(f), \tag{13}$$

where $\tau_{\mathrm{SFOAE}}(f)$ is the SFOAE phase-gradient (or group) delay. Using this estimate in Eq. (12) yields the prediction $\Delta f_{\mathrm{SOAE}}(f) \approx 1/\tau_{\mathrm{SFOAE}}(f)$, or, equivalently

$$N_{\mathrm{SOAE}}(f) \approx N_{\mathrm{SFOAE}}(f), \tag{14}$$

where $N_{\mathrm{SOAE}} \equiv \overline{f}_{\mathrm{SOAE}}/\Delta f_{\mathrm{SOAE}}$ and $N_{\mathrm{SFOAE}} = f\tau_{\mathrm{SFOAE}}$. The function $N_{\mathrm{SFOAE}}(f)$ is simply SFOAE group delay expressed in periods of the stimulus frequency (Shera and Guinan, 2003). As in Fig. 2, the frequency $\overline{f}_{\mathrm{SOAE}}$ is the geometric mean frequency of the pair of adjacent SOAEs. Equation (14) relates the frequency spacing of *spontaneous* OAEs to the group delay of *evoked* stimulus-frequency OAEs.

A. The characteristic spacing and its dependence on frequency

Figure 3 replots the histogrammed SOAE data (Fig. 2) as a scatterplot versus emission frequency.[10] The density of points is greatest in the upper part of the plot, corresponding to SOAEs separated by intervals close to the characteristic minimum spacing (e.g., $|\Delta n| = 1$). SOAEs separated by wider intervals (e.g., those corresponding to $|\Delta n| > 1$) contribute to the more diffuse appearance in the bottom half. The solid line shows a robust power-law fit, $\overline{N}_{\mathrm{SOAE}}(f)$, to the mode of the distribution. The power-law form of $\overline{N}_{\mathrm{SOAE}}(f)$ appears as a straight line on these log-log axes.

We test Eq. (14) over a four-octave frequency range in the human ear by overlaying the function $\overline{N}_{\mathrm{SFOAE}}(f)$ representing a power-law fit to measurements of human SFOAE group delay (Shera and Guinan, 2003). Agreement between $\overline{N}_{\mathrm{SOAE}}(f)$ and $\overline{N}_{\mathrm{SFOAE}}(f)$ is generally good, although the two lines are somewhat offset from one another, indicating that $1/\overline{\tau}_{\mathrm{SFOAE}}(f)$ slightly overestimates the mean characteristic spacing $\overline{\Delta f}_{\mathrm{SOAE}}(f)$. The parameters of the power-law fits quantify these conclusions (see Table I). Given the estimated uncertainties (95% confidence intervals), the offset between the lines appears significant (compare $\overline{N}_{\mathrm{SOAE}} = 13.7 \pm 0.7$ at 1 kHz versus $\overline{N}_{\mathrm{SFOAE}} = 11.1 \pm 1.2$); the power-law exponents, however, are essentially indistinguishable (compare $\alpha = 0.31 \pm 0.05$ for $\overline{N}_{\mathrm{SOAE}}$ versus $\alpha = 0.37 \pm 0.07$ for $\overline{N}_{\mathrm{SFOAE}}$).

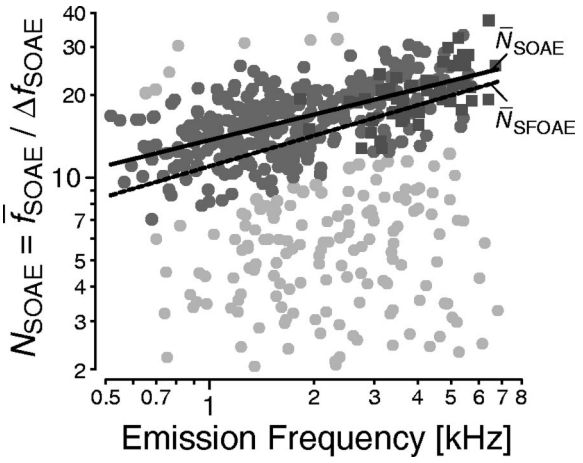

FIG. 3. SOAE spacings compared with SFOAE group delay. The SOAE data from Fig. 2 are presented as a scatterplot showing N_{SOAE} versus emission frequency, $\overline{f}_{\mathrm{SOAE}}$. The circles and squares denote the adult and infant data, respectively. The solid line shows a power-law fit, $\overline{N}_{\mathrm{SOAE}}(f)$, to the peak of the distribution (parameters in Table I). To reduce bias in the fit caused by SOAE pairs with values N_{SOAE} off the peak of the distribution (e.g., data points corresponding to values $|\Delta n| > 1$), a robust loess trend line (Cleveland, 1993) was first computed to locate the approximate mode of the distribution (the results agreed closely with a line drawn by eye). Only data points lying within two standard deviations about the trend line were then included in the fit. Points excluded from the fit are shown in light gray. For comparison, the dashed line shows the power-law fit, $\overline{N}_{\mathrm{SFOAE}}(f)$, computed from measurements of human SFOAE group delay in 9 subjects (Shera and Guinan, 2003).

1. Origins of the discrepancy

Systematic offsets between $\overline{N}_{\mathrm{SOAE}}$ and $\overline{N}_{\mathrm{SFOAE}}$ (see Fig. 3) are expected on theoretical grounds. Recall that the second term in Eq. (8) for $\theta(f)$, approximated as constant in Eq. (9), actually varies slowly with f. The two angles $\theta(f)$ and $\angle P_{\mathrm{SFOAE}}$—the first responsible for quantization of SOAE spacings, the second for SFOAE group delay—therefore rotate at somewhat different rates. The global standing-wave model thus predicts that SOAE frequency spacings generally differ somewhat from the value

TABLE I. Parameters of power-law fits to the functions $N_{\mathrm{SOAE}}(f)$ and $N_{\mathrm{SFOAE}}(f)$. The parameters $\{\alpha,\beta\}$ characterizing the frequency dependence of $N_{\mathrm{SOAE}}(f)$ and $N_{\mathrm{SFOAE}}(f)$ were determined by linear regression using power-law fits of the form $y = \beta x^\alpha$, where y is the dependent variable and $x = f/[\mathrm{kHz}]$ (i.e., frequency or characteristic frequency in kHz). The numbers in parentheses give the approximate uncertainty (i.e., 95% confidence interval) in the final digit(s) estimated from the fits [e.g., $0.31(5) = 0.31 \pm 0.05$]; when the uncertainty is 1 or greater, the position of the decimal point is shown for clarity. The uncertainties in α and $\log\beta$ are strongly correlated, with a typical correlation coefficient between them of roughly -0.8. The parameter β for $\overline{N}^*_{\mathrm{SFOAE}}(f)$ includes a rough correction for the difference in effective sound intensity (see text); the corresponding confidence interval does not include contributions from the appreciable uncertainty in the mean magnitude of round-trip middle-ear transfer functions.

	$\overline{N}_{\mathrm{SOAE}}$	$\overline{N}_{\mathrm{SFOAE}}$	$\overline{N}^*_{\mathrm{SFOAE}}$
α	0.31(5)	0.37(7)	0.37(7)
β	13.7(7)	11.1(1.2)	14.1(1.5)

$1/\overline{\tau}_{\mathrm{SFOAE}}(f)$ given by Eq. (14) (Talmadge *et al.*, 1998). Although the magnitude and sign of this difference depend on middle-ear and transducer characteristics not known with any certainty, Puria's (2003) measurements suggest that it is small (see Sec. III A), amounting to only a fraction of a period at the frequencies explored here.

Differences in the effective intracochlear sound intensities characterizing the two data sets can also produce a systematic offset between $\overline{N}_{\mathrm{SOAE}}$ and $\overline{N}_{\mathrm{SFOAE}}$. Like those shown in Fig. 1, the SFOAE group-delay measurements in Fig. 3 were made at an ear-canal sound level (40 dB SPL) sufficient to ensure that $|R| \ll 1$. SOAE amplitudes, however, are typically somewhat less than 0 dB SPL (e.g., Talmadge *et al.*, 1993). Although measurements of middle-ear transfer functions show considerable intersubject variability, they suggest that these ear-canal SOAE levels result from intracochlear sound pressures roughly the equivalent of those produced by a 15–30-dB SPL stimulus tone (Puria, 2003).[11] Since evoked-emission group delays decrease systematically with increasing sound level (Neely *et al.*, 1988), measurements of $N_{\mathrm{SFOAE}}(f)$ at 40 dB SPL are likely to underestimate values at lower, more comparable sound levels. Although the magnitude of the resulting offset is difficult to estimate with any certainty, taking the effective intracochlear sound-level difference to be roughly 15 dB yields the ''intensity-corrected'' estimate $\overline{N}^{*}_{\mathrm{SFOAE}} = 14.1 \pm 1.5$ at 1 kHz,[12] in closer agreement with the value for $\overline{N}_{\mathrm{SOAE}}$. Note that the reported confidence interval for $\overline{N}^{*}_{\mathrm{SFOAE}}$ does not include contributions from the appreciable uncertainty in the mean magnitude of round-trip middle-ear transfer functions. Despite the considerable uncertainties, this account of the discrepancy between $\overline{N}_{\mathrm{SOAE}}$ and $\overline{N}_{\mathrm{SFOAE}}$ is supported by the analysis of Zweig and Shera (1995), who found no significant difference between the mean value of Δf_{SOAE} averaged over the interval 1–2 kHz and the mean value of $1/\tau_{\mathrm{SFOAE}}$ obtained from 1–2-kHz measurements of ear-canal pressure at a stimulus level of 10 dB SPL.

2. SOAE spacings in other mammals

Although data characterizing the relation between SOAEs and evoked emissions in nonhuman mammals are extremely limited, the available evidence supports the strong correlation between $\overline{N}_{\mathrm{SOAE}}(f)$ and $\overline{N}_{\mathrm{SFOAE}}(f)$ demonstrated here in human ears (Fig. 3). OAE measurements in chinchillas, for example, yield a good correspondence between SOAE spacings and the frequency spacing characteristic of distortion-product (DPOAE) fine structure (Long *et al.*, 2000). Since theoretical and experimental work has demonstrated that DPOAE fine-structure spacing measured at fixed f_2/f_1 is largely determined by SFOAE phase (Talmadge *et al.*, 1998; Kalluri and Shera, 2001), a strong correlation between DPOAE fine structure and SOAE spacings is predicted by the global standing-wave model. Unfortunately, the fact that SOAEs detectable in chinchillas generally occur at higher frequencies than in humans complicates a direct interspecies comparison. Extrapolating the power-law form of the human $\overline{N}_{\mathrm{SOAE}}(f)$ to the chinchilla modal SOAE frequency of 10 kHz suggests that chinchilla SOAE spacings are roughly a factor of 2 larger than their counterparts in humans. This difference is consistent [cf. Eq. (14)] with the observation that human SFOAE group delays are longer, by roughly a factor of 2–3, than those in laboratory animals such as cats and guinea pigs (Shera and Guinan, 2003; Zwicker and Manley, 1981).

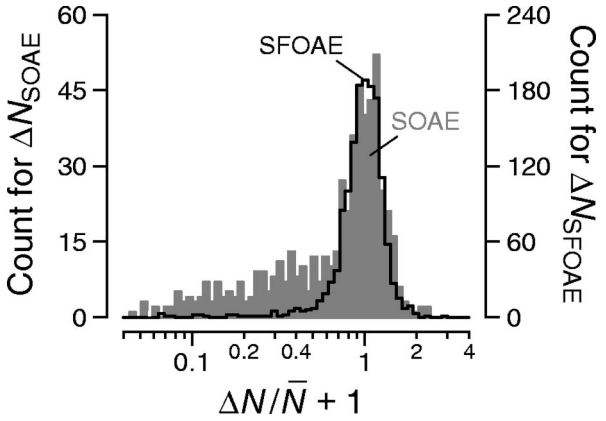

FIG. 4. Variability of SOAE spacings and SFOAE group delay. The figure shows histograms of the deviations $\Delta N_{\mathrm{SOAE}}/\overline{N}_{\mathrm{SOAE}}$ (shaded gray) and $\Delta N_{\mathrm{SFOAE}}/\overline{N}_{\mathrm{SFOAE}}$ (black line), where $\Delta N \equiv N - \overline{N}$. The deviations $\Delta N/\overline{N}$ have been pooled across frequency and are plotted on a logarithmic scale by showing the value $\Delta N/\overline{N}+1$ along the abscissa. For ΔN_{SOAE}, residuals about the power-law fit, $\overline{N}_{\mathrm{SOAE}}(f)$, were computed from the data shown in Fig. 3; the histogram is based on 556 measurements in 47 subjects. For $\Delta N_{\mathrm{SFOAE}}$, residuals about $\overline{N}_{\mathrm{SFOAE}}(f)$ were computed from the data of Shera and Guinan (2003); the histogram is based on 1441 measurements in 9 subjects. The vertical scales (left and right axes) differ by a factor of 4, a value set by the ratio of histogram areas on the interval $1 \pm \sigma$, where $\sigma \approx 0.25$ is the standard deviation of the SFOAE histogram about its peak. SOAEs spaced at wide intervals corresponding to $|\Delta n| > 1$ contribute to the long tail of the SOAE histogram that extends leftwards along the abscissa.

B. Variability of SOAE spacings

Figure 4 demonstrates that the global standing-wave model also accounts for the evident variability in the spacing of adjacent SOAEs (see Figs. 2 and 3). The figure shows histograms of the deviations $\Delta N_{\mathrm{SOAE}}/\overline{N}_{\mathrm{SOAE}}$ and $\Delta N_{\mathrm{SFOAE}}/\overline{N}_{\mathrm{SFOAE}}$, where in each case $\Delta N \equiv N - \overline{N}$. About their peaks the two distributions are nearly identical. They differ in their tails because the SOAE histogram includes data from adjacent SOAEs with wide frequency spacings. According to the global standing-wave model, SOAEs at wide spacings result from gaps in the series created by ''dropouts.'' Because of variations across frequency in the value of $|RR_{\mathrm{stapes}}|$, not all frequencies $f^{(n)}_{\mathrm{SOAE}}$ in Eq. (10) are realized as SOAEs and SOAEs separated by intervals corresponding to $|\Delta n| > 1$ often occur. The SOAE histogram is therefore skewed leftward in the tail. Despite this expected difference in the tails of the two distributions, the strong quantitative match between the peaks supports the global standing-wave model, which predicts that the variability in close SOAE spacings results from variations in $\tau_{\mathrm{SFOAE}}(f)$. The theory of coherent reflection filtering traces this variability in $\tau_{\mathrm{SFOAE}}(f)$ to the randomness of the underlying impedance perturbations filtered by properties of the traveling wave (see Sec. VII D).

C. Frequency shifts due to changes in middle-ear impedance

The standing-wave quantization condition [Eq. (5)] can be used to predict the magnitude and sign of the SOAE frequency shifts induced by changes in middle-ear impedance. To obtain the relation, we let the load impedance presented to the cochlea by the middle and external ears depend on some parameter whose unperturbed value we denote by κ. For example, κ might be the stiffness of the annular ligament or the static pressure in the ear canal. For an SOAE of frequency f the standing-wave quantization condition implies that

$$\angle R(f)+\angle R_{\text{stapes}}(f,\kappa)=2\pi n, \tag{15}$$

where κ appears among the independent variables that determine R_{stapes}. Imagine now that we modify the middle-ear load by taking $\kappa\rightarrow\kappa+\delta\kappa$. Because of the resulting change in stapes reflectance, the standing-wave quantization condition [Eq. (15)] is no longer satisfied at frequency f. To maintain the standing wave, the SOAE frequency must shift ($f\rightarrow f+\delta f$). When the equality in Eq. (15) has been restored

$$\angle R(f+\delta f)+\angle R_{\text{stapes}}(f+\delta f,\kappa+\delta\kappa)=2\pi n, \tag{16}$$

where we have assumed that all changes are small enough that n remains invariant. Equations (15) and (16) imply that the net phase change due to the combined effects of $\delta\kappa$ and δf must be zero. To first order in $\delta\kappa$ and δf

$$(\partial_f\angle R+\partial_f\angle R_{\text{stapes}})\,\delta f+(\partial_\kappa\angle R_{\text{stapes}})\,\delta\kappa=0, \tag{17}$$

where we have used the notational shorthand $\partial_x\equiv\partial/\partial x$. Since $\angle R_{\text{stapes}}$ rotates much less rapidly with frequency than $\angle R$ (i.e., $|\partial_f\angle R_{\text{stapes}}|\ll|\partial_f\angle R|$; see Sec. III A), we obtain the relation

$$\delta f\approx-\left(\frac{\partial_\kappa\angle R_{\text{stapes}}}{\partial_f\angle R}\right)\delta\kappa. \tag{18}$$

Equation (18) can be put in a form more convenient for comparison with experiment by writing it in terms of fractional changes:

$$\delta f/f\approx\left(\frac{\partial_{\ln\kappa}\angle R_{\text{stapes}}}{2\pi N_{\text{SFOAE}}}\right)\delta\kappa/\kappa, \tag{19}$$

where we have used $N_{\text{SFOAE}}\equiv f\cdot\tau_{\text{SFOAE}}$ with $\tau_{\text{SFOAE}}\approx-\partial_f\angle R/2\pi$. Equation (19) relates fractional changes in SOAE frequency to fractional changes in the middle-ear parameter κ. Note that the result is completely general and does not depend on any particular form for R_{stapes}.

1. Frequency shifts due to middle-ear stiffness changes

We can use Eq. (19) to predict the relative signs of δf and $\delta\kappa$ under manipulations that change the effective stiffness of the middle ear. We proceed by combining Eq. (19) with Puria's (2003) measurements and model of $R_{\text{stapes}}(f)$ in human temporal bones. Puria has shown that the general trends in his measurements of $R_{\text{stapes}}(f)$ are well captured by a simple model that approximates the cochlear input impedance as resistive and the middle-ear load seen from the cochlea by a series combination of spring, mass, and damper.[13]

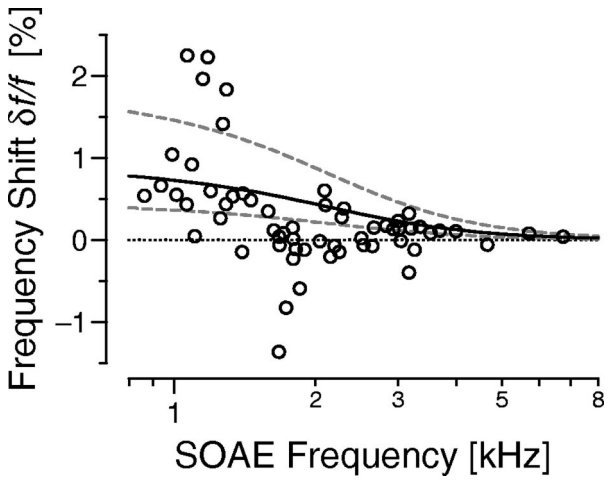

FIG. 5. Comparison of measured and predicted effect of postural changes on SOAE frequencies. Measured SOAE frequency shifts (○, 60 SOAEs from 13 ears) from the study of de Kleine *et al.* (2000) are shown together with standing-wave-model predictions based on Eq. (19), with κ taken to be the effective stiffness of the middle-ear load. The quantity $\partial_{\ln\kappa}\angle R_{\text{stapes}}$ was evaluated using Puria's (2003) simple model of $R_{\text{stapes}}(f)$; $N_{\text{SFOAE}}(f)$ was approximated by the power-law fit shown in Fig. 3. The solid line corresponds to a fractional stiffness increase $\delta\kappa/\kappa$ of 50%; the dashed lines to increases of 25% and 100% (lower and upper curves, respectively). The dotted line marks the location of the zero along the ordinate.

Using this approximation and taking κ to be the spring constant of the middle-ear load yields $\partial_{\ln\kappa}\angle R_{\text{stapes}}>0$. According to Eq. (19), δf and $\delta\kappa$ therefore have the same sign. In other words, the global standing-wave model predicts that increasing the stiffness of the middle-ear system (e.g., by tensing the eardrum or stretching the annular ligament) generally increases SOAE frequencies, in agreement with the changes observed experimentally (e.g., Kemp, 1981; Wilson and Sutton, 1981; Zurek, 1981; Schloth and Zwicker, 1983; Hauser *et al.*, 1993; de Kleine *et al.*, 2000).

2. Magnitude, sign, and frequency dependence of the shifts

Figure 5 quantifies these remarks by comparing standing-wave-model predictions with the posture-induced changes in SOAE frequencies measured by de Kleine *et al.* (2000). Equation (19) was evaluated using Puria's (2003) model of $R_{\text{stapes}}(f)$ and the power-law fit to measurements of $N_{\text{SFOAE}}(f)$ shown in Fig. 3 (Shera and Guinan, 2003). Since the magnitudes of posture-induced changes in the stiffness of the middle-ear load are not known with any certainty, and presumably vary from subject to subject depending on such things as the patency of the cochlear aqueduct, we show predictions using three different values of $\delta\kappa/\kappa$ corresponding to increases of 25%, 50%, and 100%. Estimated stiffness increases of roughly this magnitude were obtained in studies of middle-ear transmission in which the impedance of the annular ligament was varied using postural shifts (Avan *et al.*, 2000; Büki *et al.*, 2000). These estimates are also broadly consistent with the results of Pang and Peake (1986), who made direct measurements of the stiffness of the annular ligament during stapedius-muscle contractions in cat and found increases ranging up to a factor of 10; changes induced by postural shifts are likely to be significantly smaller.

Although the measured SOAE frequency shifts show considerable scatter, Fig. 5 demonstrates that the global standing-wave model [Eq. (19)] quantitatively accounts for the major features reported in the data (e.g., de Kleine *et al.*, 2000). These features include the typical magnitude of the SOAE frequency shifts (1–2%), their most common direction (toward higher frequencies), and their overall variation with SOAE frequency (largest below 2 kHz). The scatter in the data presumably results from intersubject variation and details of the middle-ear load not captured by the simple model of $R_{\text{stapes}}(f)$. For example, Puria's measurements indicate that although $\angle R_{\text{stapes}}(f)$ generally decreases over the frequency range shown in Fig. 5, the change is not perfectly smooth. Unlike the model, the data manifest considerable local variation in the magnitude and sign of the phase slope. These local departures from the overall trend are presumably responsible for much of the observed variation in SOAE frequency shifts (e.g., the decrease in SOAE frequencies near 2 kHz).

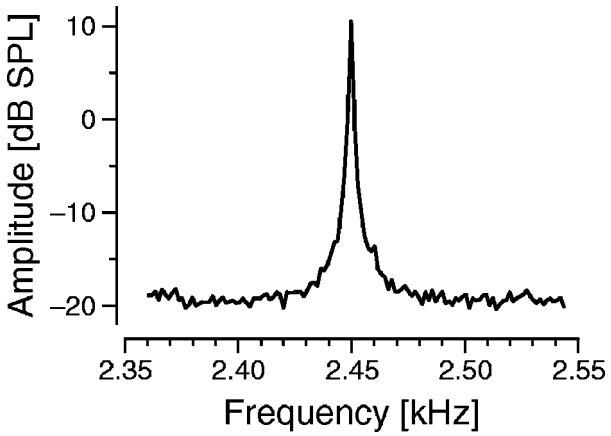

FIG. 6. Frequency spectrum for a typical human SOAE. The figure shows the spectrum obtained by averaging the spectral amplitudes of 89 contiguous segments of SOAE waveform, each of approximately 671 ms duration (subject WL-R). The total averaging time was about 60 seconds. Measurement methods are described in footnote 14.

3. Middle-ear contributions to emission bandwidths

Although we have focused here on artificially induced changes in middle-ear impedance, continuous small perturbations in the basal boundary condition presumably occur naturally from a number of sources, including variations in middle-ear cavity pressures due to breathing, swallowing, or blood flow; variations in the stiffness of the annular ligament due to spontaneous stapedius contractions; and changes in intracochlear pressure related to heartbeat. According to the global standing-wave model, these and other ongoing physiological perturbations produce small corresponding fluctuations in SOAE frequencies. Equation (19) relating $\delta f/f$ to changes $\delta\kappa/\kappa$, where κ can be any parameter that modifies $\angle R_{\text{stapes}}$, predicts that fractional SOAE frequency shifts are inversely proportional to N_{SFOAE}. In other words, the longer the SFOAE group delay [i.e., the more rapidly $\angle R(f)$ rotates with frequency], the more stable are SOAE frequencies against perturbations in the boundary conditions. All other things being equal, the global standing-wave model thus predicts that species with long SFOAE group delays should generally have more stable SOAEs (i.e., narrower SOAE bandwidths) than species with shorter delays. Interestingly, this is precisely the trend observed experimentally (e.g., Ohyama *et al.*, 1991; Long *et al.*, 2000): SOAEs in guinea pigs and chinchillas, species with relatively short group delays, are generally less stable and have broader bandwidths than SOAEs in humans, where SFOAE group delays are substantially longer (Shera and Guinan, 2003).

VI. ARE THE STANDING WAVES POWERED BY NOISE?

Most global standing-wave models in the literature propose that mammalian SOAEs—such as the one whose spectrum is illustrated in Fig. 6—result from intracochlear standing waves stabilized by a balance between round-trip energy losses and level-dependent coherent wave amplification. Nevertheless, standing-wave resonances driven solely by thermal or other noise sources would also appear as narrow-band acoustic signals in the ear canal (Allen and Fahey, 1992; Allen, 2001). If the standing-wave resonances were of sufficiently high Q, the ear-canal spectral characteristics of the SOAEs generated by a ''passive,'' noise-driven standing-wave model would be indistinguishable from the amplitude-stabilized coherent signals produced by the ''active'' standing-wave model.

A. Generalization of the Bialek–Wit histogram

Although they cannot be distinguished by their spectra, the acoustic signals generated by the two different models (i.e., narrow-band filtered noise versus amplitude-stabilized oscillations) can be distinguished by the statistical properties of their time waveforms, as Bialek and Wit (1984) were the first to point out for SOAEs. Bialek and Wit showed that the SOAE pressure waveform has a double-humped, non-Gaussian probability distribution inconsistent with the output of a linear passive narrow-band filter driven by noise. Talmadge *et al.* (1991) subsequently showed that double-humped distributions rule out many nonlinear passive systems as well. Here, we extend the Bialek–Wit analysis to explicitly demonstrate the amplitude stabilization that distinguishes SOAEs from narrow-band filtered noise. The Bialek–Wit histogram is a one-dimensional projection of the more general two-dimensional distribution described here.

To obtain the distribution, we begin by writing the time-varying ear-canal pressure due to an SOAE in the form

$$p_{\text{SOAE}}(t) = p(t)\cos[2\pi f_{\text{SOAE}} t + \phi(t)], \tag{20}$$

where f_{SOAE} is the nominal SOAE frequency and $p(t)$ and $\phi(t)$ are its slowly varying amplitude and phase. We then represent the SOAE waveform by the complex phasor

$$\tilde{p}_{\text{SOAE}}(t) \equiv p(t)e^{i\phi(t)}. \tag{21}$$

Over time, the phasor $\tilde{p}_{\text{SOAE}}(t)$ moves about in the complex plane, tracing out a trajectory whose instantaneous polar coordinates (i.e., radial distance from the origin and angle with the real axis) are $p(t)$ and $\phi(t)$, respectively. The real and imaginary parts of $\tilde{p}_{\text{SOAE}}(t)$ are thus the in-phase and

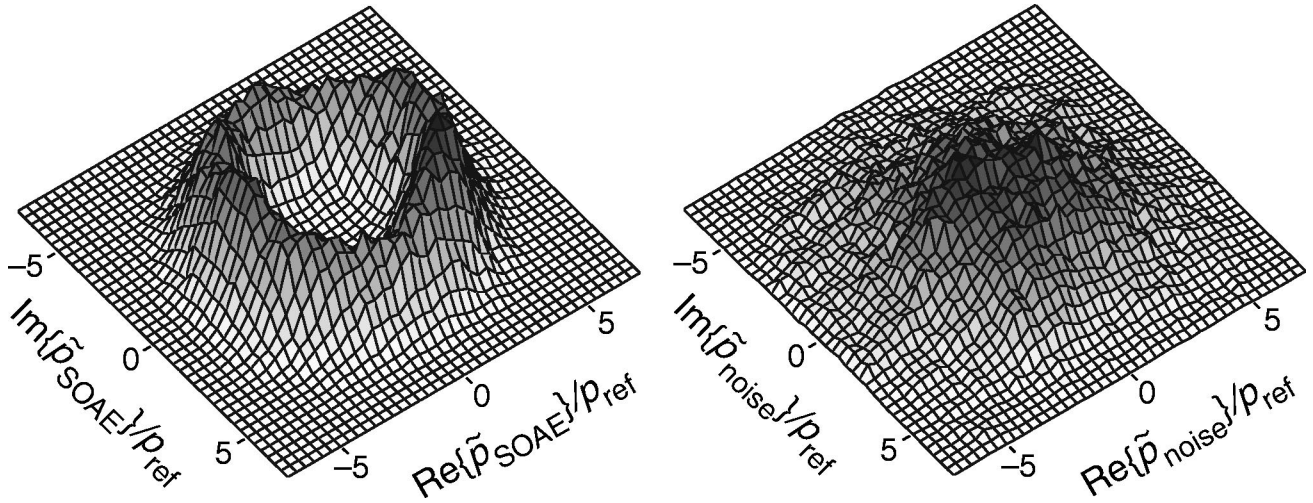

FIG. 7. Probability distributions $\mathcal{D}[\tilde{p}_{\mathrm{SOAE}}(t)]$ and $\mathcal{D}[\tilde{p}_{\mathrm{noise}}(t)]$ for an SOAE and for a narrow-band noise signal with the same power spectrum. Distributions were computed from 80 s of data as described in footnote 14 for the human SOAE shown in Fig. 6 (left-hand panel) and a noise signal with the identical power spectrum (right-hand panel). The x- and y axes represent the real and imaginary parts (in-phase and quadrature components) of the complex phasors $\tilde{p}(t)$ described in the text. Pressures are shown in units of $p_{\mathrm{ref}}=20\ \mu$Pa.

quadrature components obtained by heterodyning the SOAE waveform using a reference signal of frequency f_{SOAE}.

B. Molehills and moleruns

Figure 7 (left-hand panel) gives the probability distribution $\mathcal{D}_{\mathrm{S}}\equiv\mathcal{D}[\tilde{p}_{\mathrm{SOAE}}(t)]$ obtained from the SOAE shown in Fig. 6.[14] For comparison, and as a control, the right-hand panel gives the corresponding distribution, $\mathcal{D}_{\mathrm{N}}\equiv\mathcal{D}[\tilde{p}_{\mathrm{noise}}(t)]$, for a noise signal filtered in such a way that its power spectrum is identical to that of the SOAE. [The noise signal was obtained by passing random-phase, flat-spectrum noise through a filter with frequency response equal to the amplitude spectrum of the SOAE, as illustrated in Fig. 6. The phasor $\tilde{p}_{\mathrm{noise}}(t)$ was subsequently computed as described for $\tilde{p}_{\mathrm{SOAE}}(t)$ in footnote 14.] Both distributions are shown as functions of the complex variable $\tilde{p}$. In other words, the x and y axes give the possible amplitudes of the $\cos(2\pi f_{\mathrm{SOAE}}t)$ and $\sin(2\pi f_{\mathrm{SOAE}}t)$ components of the signal. The height of the surface above any small element of area in the plane is proportional to the long-term average probability that the in-phase and quadrature components of the signal, as measured during any particular short interval of time, will be found to lie within the specified range.

For the filtered-noise signal, the phasor $\tilde{p}_{\mathrm{noise}}(t)$ wanders randomly about in the complex plane at a rate inversely proportional to the signal bandwidth. This random motion appears superimposed on a circular drift whose angular velocity is proportional to the difference between the instantaneous signal frequency and the center frequency of the spectrum. The resulting probability distribution, $\mathcal{D}_{\mathrm{N}}$, is that of a two-dimensional Gaussian ''molehill'' centered on the origin (Rice, 1954).

As illustrated in Fig. 7, the statistics of the SOAE signal are strikingly different from filtered noise. Rather than resembling a molehill, the probability distribution suggests a ''molerun'' or volcanic caldera. Near the origin, where $\mathcal{D}_{\mathrm{N}}$ is largest, $\mathcal{D}_{\mathrm{S}}$ is vanishingly small. Significant values of $\mathcal{D}_{\mathrm{S}}$ are confined to a relatively narrow ring of finite radius. Evidently, the SOAE amplitude is stabilized at a nonzero value about which it manifests only small fluctuations (e.g., due to thermal noise and other physiological perturbations). SOAE phase, by contrast, exhibits no such stabilization; over time, the phase wanders through all possible angles, its random motion again superimposed on a circular drift whose speed and direction change erratically according to the magnitude and sign of transient deviations in SOAE frequency about its central value.[15] Although the absolute phase reference necessary to stabilize SOAE phase is not available physiologically, phase stabilization can be achieved by entraining the emission to an external tone.

Projecting the caldera-like distribution $\mathcal{D}_{\mathrm{S}}$ shown in the left-hand panel of Fig. 7 onto the xz plane (i.e., computing the distribution $\mathcal{D}[\mathrm{Re}\{\tilde{p}_{\mathrm{SOAE}}(t)\}]$) yields a double-humped, non-Gaussian histogram similar to those reported previously in mammals, lizards, and birds (e.g., Bialek and Wit, 1984; Talmadge *et al.*, 1991; van Dijk *et al.*, 1996).[16] Unlike the Bialek–Wit distribution, however, the caldera $\mathcal{D}_{\mathrm{S}}$ clearly demonstrates that fluctuations in SOAE amplitude are limited both from above and from below [see also Fig. 3 of Talmadge *et al.* (1991)]. SOAEs amplitudes are evidently stabilized within a narrow range and, in particular, almost never fall appreciably below their mean value. Although amplitude stabilization of this sort can readily be understood in the context of the active standing-wave model (see Sec. VII A), it appears difficult if not impossible to reconcile with the passive standing-wave model and its assumption that SOAEs are powered entirely by randomly fluctuating, incoherent biological noise.

VII. DISCUSSION

Our quantitative tests provide strong support for the global standing-wave model and its prediction that SOAE frequencies are determined by RR_{stapes} (e.g., Kemp, 1979a, b; Zweig and Shera, 1995; Talmadge *et al.*, 1998). The results demonstrate that in addition to predicting the existence of multiple emissions with a characteristic minimum frequency

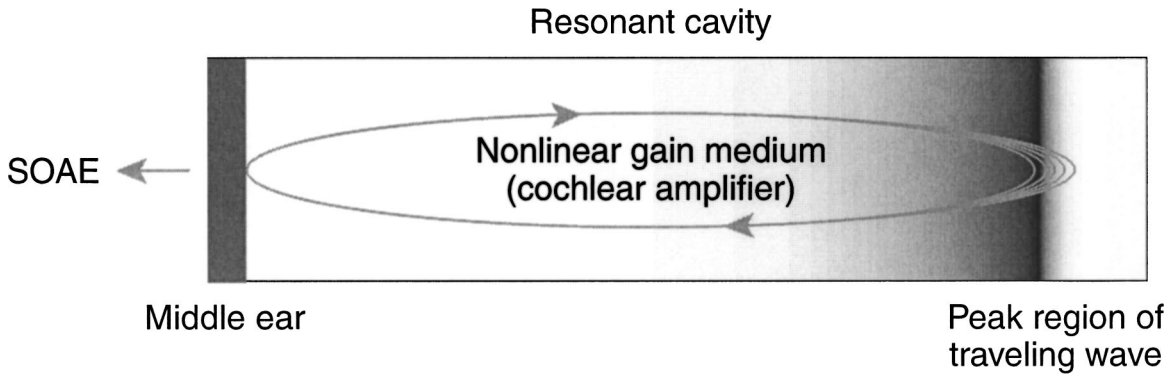

FIG. 8. Analogy between the cochlear production of SOAEs and the coherent emission of light by an optical laser. The region between the stapes and the peak of the traveling wave is represented as a resonant cavity enclosing a nonlinear gain medium. The gradient in shading illustrates that most of the amplification occurs just basal to the peak of the traveling wave. Partial reflection of forward- and backward-traveling waves occurs at each end of the cavity. At the apical end, coherent reflection occurs over a distributed region spanning the peak of the traveling wave. Standing waves occur at frequencies for which the round-trip phase change is an integral multiple of 2π. Standing-wave amplitudes are stabilized when the round-trip gain matches the round-trip losses due to internal damping and acoustic emission through the middle ear into the environment.

spacing, the global standing-wave model also accurately predicts the mean value of this spacing, its standard deviation, and its power-law dependence on SOAE frequency. Furthermore, the global standing-wave model accounts for the magnitude, sign, and frequency dependence of changes in SOAE frequency that result from modulations in middle-ear stiffness. Although some of the SOAE characteristics tested and accounted for here might be replicable in artfully constructed local-oscillator models (e.g., by *ad hoc* adjustment of SOAE spacings), they all arise quite naturally and immediately in the global standing-wave framework. Finally, the statistics of SOAE time waveforms demonstrate that SOAEs are coherent, amplitude-stabilized signals. Taken together, these tests of the global standing-wave model support the proposed mechanism-based classification of SOAEs within the group of reflection-source OAEs (Shera and Guinan, 1999). In addition, they provide compelling evidence that mammalian SOAEs constitute a global collective phenomenon—amplitude-stabilized cochlear standing waves—rather than the local, autonomous oscillation of some cellular constituent of the organ of Corti.

A. Analogy with a laser oscillator

The existence of amplitude-stabilized standing waves within the cochlea suggests that the cochlea is acting as a biological, hydromechanical analog of a laser oscillator (see also Zweig, 1991; Russell and Kössl, 1999; Kemp, 2002). Reduced to its essentials, a laser oscillator consists of a resonant cavity enclosing a gain medium that supports coherent wave amplification (see Fig. 8). In the cochlea, the ''resonant cavity'' spans the region between the stapes and the peak of the traveling wave. At either end of this region, cochlear traveling waves are partially reflected back into the cavity. At the stapes, backward-traveling waves reflect due to the impedance mismatch with the middle ear; at the apical end of the cavity, forward-traveling waves undergo coherent reflection near the peak of the traveling wave. With partially reflecting ''mirrors'' at both ends, the cochlea differs from a typical optical laser, in which one of the mirrors is made perfectly reflecting. In further contrast with an optical laser, where reflection back into the cavity occurs at a well-defined location (i.e., in the plane of the reflecting mirror), the coherent reflection near the peak of the traveling wave is distributed over a finite region of the cochlea (i.e., the width of the traveling-wave envelope). The cochlear gain medium consists of the cellular force generators and surrounding mechanical, hydrodynamic, and electrical processes known collectively as the ''cochlear amplifier.'' In contrast to an optical laser, where amplification occurs uniformly throughout the cavity, amplification in the cochlea occurs almost entirely near the apical mirror (i.e., in the region just basal to the peak of the traveling wave).

On each pass through the cavity, waves are amplified by their interaction with the gain medium. At certain special frequencies—those for which the round-trip phase change is an integral multiple of 2π—multiple internal reflection creates standing waves. If the round-trip gain matches the round-trip losses (e.g., due to damping and acoustic radiation into the environment), stable oscillations can result that appear in the ear canal as SOAEs. Just as in an optical laser, oscillation amplitudes are self-stabilizing. Since the cochlear amplifier is limited in the energy it can produce, the gain medium is nonlinear, with the amount of amplification decreasing as the wave amplitude grows. Standing-wave amplitudes are therefore stable against perturbations: If some random fluctuation increases the wave amplitude slightly, the round-trip gain decreases a little and the wave amplitude falls back down. Conversely, if the wave amplitude decreases, the total gain increases, pulling the oscillation amplitude back up. Amplitude stabilization of this sort produces SOAE signals with the statistical properties illustrated in Fig. 7. Similar probability distributions characterize the coherent radiation generated by optical lasers (e.g., Golay, 1961; Siegman, 1986).

Unlike optical lasers, the cochlea can emit at multiple, nonharmonically related frequencies. In an optical laser, the cavity size is fixed and tuned to a single frequency and its harmonics. Wave propagation in the cochlea, however, is highly dispersive and the location of the wave peak—and hence the location of the partially reflecting mirror—depends on frequency. Consequently, the round-trip phase condition

is satisfied at many frequencies and the cochlea can produce multiple SOAEs simultaneously.

B. Sources of initial traveling-wave energy

The global standing-wave model indicates that the multiple internal reflection and amplification of traveling-wave energy responsible for SOAEs can be initiated simply by sounds from the environment and/or by physiological noise. In addition, autonomous oscillations of cells or subcellular structures may sometimes kick-start the emission process by acting as initial generators of traveling-wave energy. For example, should some ''resonant element'' within the cochlea suddenly begin to oscillate mechanically, the resulting movements presumably create backward-traveling waves (if the oscillation frequency is less than or equal to the local CF). These backward-traveling waves subsequently reflect off the stapes, thereby initiating the process of multiple internal reflection characteristic of global standing-wave resonances.

Even though the original disturbance may arise through the action of some local oscillator, long-term stability requires that any final SOAE frequency be consistent with Eq. (5), so that round-trip phase shifts equal an integral multiple of 2π. Unless the initiating oscillator can adapt by changing its frequency to satisfy this global constraint (or is largely impervious to the perturbing influence of its own energy, which is fed back to it by reflection off the stapes),[17] the oscillator's output will be highly unstable and unlikely to persist. Computational studies of ''completely active'' cochlear models consisting of an array of coupled van der Pol oscillators confirm the importance of cochlear standing waves and the middle-ear boundary condition in determining SOAE frequencies (van Hengel *et al.*, 1996).

C. Relationship to phenomenological oscillator models

Properties of SOAEs such as their interactions with one another and with external tones have been successfully described by representing individual SOAEs using a nonlinear, limit-cycle oscillator such as the van der Pol (e.g., Murphy *et al.*, 1995a, b, 1996; van Dijk and Wit, 1990a, b). These phenomenological, limit-cycle oscillator models were not, as a rule, developed to describe the ''oscillating elements'' within the cochlea; rather, their aim was to approximate the behavior of a complex system of equations (such as those describing the generation of standing waves in an active, nonlinear transmission line) by a single effective oscillator, thereby providing simple, analytically tractable representations of SOAEs as they appear in the ear canal. Thus, these phenomenological models are not inconsistent with the global standing-wave model, which proposes a mechanism by which SOAEs originate within the cochlea. The evident success of the global standing-wave model contradicts the notion, often implicit in the local-oscillator framework, that SOAEs measured in the ear canal provide direct access to the local elementary cellular oscillators within the organ of Corti (e.g., Sisto and Moleti, 1999).

D. The mechanism of reflection within the cochlea

According to the global standing-wave model, SOAEs are simply a special case of a more general and ubiquitous otoacoustic phenomenon: the production of reflection-source OAEs by the ear. Although many predictions of the model depend only on the empirical form of the cochlear traveling-wave reflectance, $R(f)$, understanding the mechanism by which reflection-source OAEs (such as low-level stimulus-frequency and transient-evoked emissions) originate provides deeper insight.

Considerable evidence suggests that the generation of reflection-source OAEs is well described by the theory of coherent reflection filtering (Shera and Zweig, 1993b; Zweig and Shera, 1995; Talmadge *et al.*, 1998; Shera and Guinan, 2003). The theory indicates that reflection-source OAEs arise via coherent reflection from densely and randomly distributed impedance perturbations. These perturbations presumably include both those clearly visible in the anatomy, such as spatial variations in outer-hair-cell (OHC) number and geometry (e.g., Engström *et al.*, 1966; Bredberg, 1968; Wright, 1984; Lonsbury-Martin *et al.*, 1988), as well as morphologically less conspicuous perturbations, such as variations in OHC forces due to random, cell-to-cell variations in hair-bundle stiffness or the number of somatic motor proteins.

The coherent-reflection model predicts that the SFOAE evoked by a tone comprises a sum of wavelets scattered by perturbations located throughout the peak of the traveling wave. The SFOAE therefore arises from a distributed region, roughly equal in extent to the width of the traveling-wave envelope. In the 1–2-kHz region of the human cochlea, this distance spans on the order of 100 rows of outer hair cells at sound levels near threshold (Zweig and Shera, 1995). Although Kemp's (1979b) original standing-wave model postulated that the backward-traveling wave originates from a point reflection, the coherent-reflection model indicates that this wave necessarily arises over a region equivalent to the span of many hair cells.[18]

The theory of coherent-reflection filtering resolves other problems with the original standing-wave model. For example, Kemp (1979b) pointed out that an ''apparently random dependence [of the amplitude of the reflectance] on frequency for each ear ... is necessary to account for the presence of strong resonances at some frequencies and not others.'' The coherent-reflection model explains this random variation in reflectance magnitude by representing the total backward wave as the sum of many wavelets having an irregular distribution of amplitudes and phases dependent on the particular array of impedance perturbations encountered within the peak of the traveling wave. This same mechanism also produces random variations in reflectance phase over frequency, giving rise to the distribution of SOAE spacings about their mean value (Fig. 4).

According to the coherent-reflection theory, quantitative features of the distribution of SOAE spacings such as its central value and relative spread are determined dynamically by properties of the traveling wave (Zweig and Shera, 1995; Talmadge *et al.*, 1998). For example, the characteristic mini-

mum spacing at frequency f is set by the value of the wavelength, $\hat{\lambda}$, near the peak of the wave envelope:

$$\overline{N}_{\mathrm{SOAE}}(f) \approx \overline{N}_{\mathrm{SFOAE}}(f) \approx 2N_{\mathrm{BM}}(f), \tag{22}$$

where

$$N_{\mathrm{BM}} = l/\hat{\lambda}, \tag{23}$$

and is a function of location (or characteristic frequency) within the cochlea.[19] In these equations the parameter l represents the distance over which the characteristic frequency (CF) changes by a factor of e, and the factor of 2 originates in round-trip phase shifts and the Bragg scattering condition. According to the theory, the observed increase in the value of $\overline{N}_{\mathrm{SOAE}}$ towards the base of the cochlea (Fig. 3) reflects the systematic decrease in the wavelength $\hat{\lambda}$, which diminishes at a rate of roughly 25% per octave with increasing CF (Shera and Guinan, 2003).

Since Kemp's (1979b) original standing-wave model did not include the effects of traveling-wave propagation gains and/or losses,[20] the model needed to associate large reflection coefficients with many points along the basilar membrane (at a minimum, those corresponding to SOAE frequencies) in order to generate sizable standing waves. In the coherent-reflection model, by contrast, cochlear traveling waves are amplified as they propagate toward and away from the site of scattering; values of $|R|>1$ measured at the stapes are therefore readily obtained with only small perturbations in the mechanics (Talmadge and Tubis, 1993; Zweig and Shera, 1995). Since small, densely distributed perturbations can produce large values of $|R|$, the modern standing-wave model predicts that most SOAEs result from normal mechanical variability rather than from pathologically large impedance discontinuities. [A possible exception may be the relatively rare class of ''atypical SOAEs'' characterized by their unusually large amplitudes and frequent association with significant audiometric abnormality (reviewed in Lonsbury-Martin and Martin, 2001).]

In contrast to the local-oscillator model, which typically emphasizes the pathology of the condition by ascribing SOAEs to a ''disturbance'' or outright ''failure'' of some local feedback control mechanism, the global standing-wave model emphasizes the *normality* of most SOAEs by demonstrating both their close relation to other types of evoked OAEs (i.e., low-level SFOAEs and other reflection-source emissions) and their origin as the expected consequence of distributed wave amplification and reflection in the presence of small, nonpathological impedance perturbations. In this way, the global standing-wave model resolves the paradox noted by Geisler (1998) in his discussion of the van der Pol oscillator as a local-oscillator model for SOAEs:

> ''[Why] doesn't every section of the cochlea act that way [i.e., as a limit-cycle oscillator] and [the cochlea therefore] produce emissions at all frequencies? It follows that there must be something different about those cochlear sites that generate the relatively few emissions observed. Unfortunately, the search for such differences has not been successful.''

Viewed from the perspective of the global standing-wave model, the failure of this search for differences is not surprising. Indeed, cochlear sites corresponding to SOAE frequencies need manifest no special distinguishing features. In the global standing-wave model, SOAE frequencies are determined by RR_{stapes}, and SOAEs therefore trace their origin to aspects of the mechanics as subtle—and as *nonlocal* to the site in question—as the magnitude and angle of the impedance mismatch at the cochlear boundary with the middle ear, the spatial-frequency content of the cochlear impedance perturbations that scatter the wave, and the total round-trip traveling-wave gain and phase shift experienced en route.

E. Representations of the characteristic minimum spacing

SOAE frequency spacings are conventionally displayed using a histogram that masks any frequency dependence in the data (e.g., Fig. 2). As a result, the characteristic minimum spacing, $\overline{\Delta f}_{\mathrm{SOAE}}$, has been somewhat misrepresented in the literature. We note, for example, that the frequency dependence of $\overline{N}_{\mathrm{SOAE}}(\overline{f}_{\mathrm{SOAE}})$ evident in the scatterplot of Fig. 3 demonstrates that $\overline{\Delta f}_{\mathrm{SOAE}}$ corresponds neither to a constant fraction of an octave, to a constant distance along the basilar membrane, nor to a constant fraction of the psychophysical critical band measured in Barks (e.g., Zwicker, 1989; Russell, 1992; Talmadge *et al.*, 1993; Braun, 1997).

Although the human characteristic spacing $\overline{\Delta f}_{\mathrm{SOAE}}(f)$ bears no simple relationship to Zwicker's critical band rate scale [contrary to folklore in the field, $\overline{\Delta f}_{\mathrm{SOAE}}(f) \neq 0.4$ Bark], the spacing $\overline{\Delta f}_{\mathrm{SOAE}}(f)$ does roughly correspond to a constant fraction of the equivalent rectangular bandwidth (ERB) estimated from otoacoustic and behavioral measurements at frequencies greater than 1 kHz (Shera *et al.*, 2002; Oxenham and Shera, 2003). Using the power-law approximations to $\overline{\Delta f}_{\mathrm{SOAE}}(f)$ and $\mathrm{ERB}(f)$ [Table I and Shera *et al.* (2002)] yields $\overline{\Delta f}_{\mathrm{SOAE}}(f) \approx \beta(f/[\mathrm{kHz}])^{\alpha} \cdot \mathrm{ERB}(f)$, where $\beta = 0.93 \pm 0.08$ and $\alpha = -0.01 \pm 0.08$. Note that the power-law exponent is indistinguishable from zero. The approximate proportionality between $\overline{\Delta f}_{\mathrm{SOAE}}$ and the psychophysical ERB demonstrated here should not be taken to imply some direct causal connection between human cochlear tuning and SOAE spacings. According to the global standing-wave model and the theory of coherent reflection filtering, the proportionality arises because both SFOAE phase slopes (and hence SOAE spacings) and the bandwidths of peripheral auditory filters are, for very different reasons, strongly correlated to the group delays of basilar-membrane transfer functions (Shera and Guinan, 2003).

We emphasize that $\overline{\Delta f}_{\mathrm{SOAE}}$ is merely the mode of a distribution of spacings and therefore has no absolute significance; inappropriate reification of its value can lead to dubious conclusions. Braun (1997), for example, argues against the global standing-wave model in order to propose an ostensible connection, mediated via efferent feedback from the inferior colliculus, between SOAE spacings and psychophysical critical bands. Braun proceeds by plotting the distribution of spacings computed from all possible SOAE pairs (i.e., an all-order distribution rather than the distribution of

first-order intervals computed from adjacent SOAEs as in Fig. 2) The all-order distribution shows only weak or nonexistent peaks at multiples of the characteristic minimum spacing $\overline{\Delta f}_{\mathrm{SOAE}}$ (which he calls the ''preferred minimum distance,'' or PMD). Braun concludes that the ''total lack of any system of multiples of the PMD in the interval distribution curve contradicts all concepts that assume a spectral periodicity of SOAEs.'' Braun's argument, however, neglects both the frequency dependence of $\overline{\Delta f}_{\mathrm{SOAE}}(f)$ and the substantial variability in the distribution of first-order intervals at fixed frequency (see Fig. 3). Because adjacent intervals are largely independent of one another, the nonzero width of the first-order distribution (see Fig. 4) smears out the distribution of higher-order intervals. For example, the distribution of second-order intervals can be approximated by convolving the first-order distribution with itself and is therefore broader than the first-order distribution by roughly a factor of 2. As a result of this smearing, peaks corresponding to higher-order intervals are difficult or impossible to discern in the all-order histogram.

1. The corresponding length scale

The spatial distance along the basilar membrane that corresponds to the modal frequency spacing $\overline{\Delta f}_{\mathrm{SOAE}}(f_{\mathrm{SOAE}})$ can be found as a function of SOAE frequency by noting that exponential position–frequency functions map constant distances Δx to constant relative frequency intervals $\Delta f/f$. According to Table I, $\overline{N}_{\mathrm{SOAE}}(\overline{f}_{\mathrm{SOAE}})=\overline{f}_{\mathrm{SOAE}}/\overline{\Delta f}_{\mathrm{SOAE}}$ varies with emission frequency as $\overline{f}^{\alpha}_{\mathrm{SOAE}}$ with $\alpha\approx 0.31\pm 0.05$; if the human cochlear map is exponential (Greenwood, 1990), the distance $\overline{\Delta x}_{\mathrm{SOAE}}$ corresponding to $\overline{\Delta f}_{\mathrm{SOAE}}$ therefore varies as $1/\overline{f}^{\alpha}_{\mathrm{SOAE}}$.

We can relate the distance $\overline{\Delta x}_{\mathrm{SOAE}}$ to the wavelength, $\hat{\lambda}$, of the traveling wave at its peak by combining these results with Eqs. (22) and (23). The calculation yields

$$\overline{\Delta x}_{\mathrm{SOAE}}\approx \tfrac{1}{2}\hat{\lambda}. \tag{24}$$

In other words, the characteristic places associated with nearest-neighbor SOAEs are separated, on average, by a distance equal to one-half the wavelength of the traveling wave. According to the coherent-reflection theory, variations about this modal value occur not because $\hat{\lambda}$ varies irregularly with position, but because the distribution of frequency spacings Δf_{SOAE} reflects an underlying disorder in the process that creates backward-traveling waves by reversing the forward flow of traveling-wave energy (i.e., scattering by random impedance perturbations). For clarity, we emphasize that the coherent-reflection theory predicts that the length scale $\overline{\Delta x}_{\mathrm{SOAE}}$ arises dynamically and need have no geometric correlate in the structure or mechanics of the cochlea (Zweig and Shera, 1995).

F. Strategies for testing the standing-wave model

The principal distinguishing prediction of the global standing-wave model is that SOAE frequencies are determined by RR_{stapes}. Specifically, the model predicts that SOAE frequencies f_{SOAE} satisfy the standing-wave quantization-condition [Eq. (5)], which requires that RR_{stapes} be positive real; equivalently

$$\theta(f_{\mathrm{SOAE}})=0 \pmod{2\pi}, \tag{25}$$

where $\theta(f)\equiv\angle\{RR_{\mathrm{stapes}}\}$. Direct experimental confirmation (or refutation) of Eq. (25) would provide a definitive test of the global standing-wave model. Unfortunately, although possible in principle, this test is difficult in practice. Rigorous tests of Eq. (25) require measurement of both $\angle R(f)$ and $\angle R_{\mathrm{stapes}}(f)$ at SOAE frequencies in a single ear. Furthermore, in the case of $\angle R(f)$, the measurement must be made at intracochlear sound intensities equivalent to those normally produced by the SOAEs in question. One is then left in the unfortunate position that the very SOAEs one is trying to understand ineluctably compromise and contaminate the measurements of $\angle R(f)$ needed to test the theory.[21]

Our strategy in this paper has been to recast the model predictions of Eq. (25) in a theoretically less definitive but experimentally more tractable form. Rather than probe the absolute phase of RR_{stapes} at frequencies f_{SOAE}, we examine the distribution of human SOAE spacings by using noninvasive measurements of SFOAEs to estimate the frequency dependence of $\angle R(f)$ and measurements of middle-ear pressure transfer functions (Puria, 2003) to argue that middle-ear contributions to the distribution of spacings Δf_{SOAE} are generally small, at least in human ears. The results provide strong but indirect support for Eq. (25) in humans (see Figs. 2–4). In addition, we use the standing-wave quantization condition to predict the effect of changes in middle-ear boundary conditions on SOAE frequencies. Although incomplete knowledge of both $\angle R_{\mathrm{stapes}}(f)$ and the magnitude of posture-induced stiffness changes in individual ears precludes a more rigorous comparison with experiment, the global standing-wave model successfully reproduces the major trends in the data (Fig. 5).

Despite their inherent limitations, our tests provide strong support for the idea that human SOAEs arise via global standing-wave resonances. Although definitive examination of the standing-wave model awaits a direct experimental probe of Eq. (25), extending the measurements and ideas developed here to SOAEs in other species, mammalian and nonmammalian alike, would provide important tests of the generality of the model.

G. SOAEs in nonmammals

Although the evidence reported here suggests that most mammalian SOAEs are amplitude-stabilized standing waves, local autonomous oscillation of some cellular constituent of the ear may, of course, underlie some subset of mammalian SOAEs (e.g., the ''atypical SOAEs'' mentioned above). The local-oscillator mechanism may also operate in species such as frogs, lizards, and birds, in which spontaneous cellular oscillations have been observed (e.g., Crawford and Fettiplace, 1985; Denk and Webb, 1992; Martin *et al.*, 2001) but which appear to lack basilar-membrane traveling waves (e.g., Peake and Ling, 1980; Manley, 1990).

Even in these species, however, we conjecture that mechanisms analogous to those posited by the global standing-wave model may often be operating. Note, for example, that the frequency selectivity of primary auditory afferent fibers in some bird and lizard species can evidently match or exceed that found in many mammalian cochleae at comparable frequencies (Manley, 2001), and associated with this tuning are substantial frequency-dependent group delays (e.g., Hillery and Narins, 1984; Smolders and Klinke, 1986; Gleich and Narins, 1988; Manley *et al.*, 1990). If frequency tuning in these species arises or is manifest mechanically, one expects significant mechanical group delays—and thus the possibility of global standing-wave-like resonances—despite the apparent absence of a clear analog of the basilar-membrane traveling wave. Although the phase changes associated with frequency tuning appear inextricably linked to basilar-membrane motion in the mammalian cochlea, the global standing-wave model imposes no such requirement. A ''resonant cavity'' containing a nonlinear ''gain medium''—comprising in this context a slightly irregular array of tuned oscillators, all coupled together through the surrounding fluids and/or via ancillary structures (e.g., the tectorial membrane) to produce the large mechanical phase shifts concomitant with sharp tuning—may be all that's required for creating global resonances analogous to those evidently responsible for SOAEs in the mammalian ear.

A common origin in global, standing-wave-like resonances may account for many of the otherwise puzzling similarities among mammalian and nonmammalian SOAEs. For example, in humans and lizards the frequency spacing between multiple SOAEs appears roughly comparable (within a factor of 2 or 3), even though the human organ of Corti is roughly 17–170 times longer than lizard papillae in overall length (Manley, 1990, 2001). The global standing-wave model explains this seemingly paradoxical observation by implying that the length of the hearing organ is essentially irrelevant to the generation of SOAEs. In the global standing-wave model, SOAE spacings are determined not by the cochlear distance between putative ''oscillating elements'' but by the frequency dependence of mechanical phase shifts; that is, by the characteristics of mechanical tuning, a functional arena where the differences between humans and lizards are less pronounced than in the anatomy (Manley, 2001). To understand more clearly the similarities and differences between mammalian and nonmammalian SOAEs, one needs to extend the types of measurements used here (e.g., determination of quantitative relationships between evoked and spontaneous OAEs and their modulation by changes in external boundary conditions) to the nonmammalian ear.

H. Implications for the cellular basis of the cochlear amplifier

The local-oscillator model of SOAEs plays a central role in recent discussions of the cellular basis of the mammalian cochlear amplifier. For example, Hudspeth and colleagues (e.g., Hudspeth, 1997; Martin and Hudspeth, 1999; Eguíluz *et al.*, 2000; Martin and Hudspeth, 2001; Martin *et al.*, 2001, 2003; Jülicher *et al.*, 2003) argue that the cellular constituents of the ear's amplifier operate near a ''critical point'' (specifically, near a so-called Andronov–Hopf bifurcation)[22] where spontaneous cellular oscillation sets in. In this view, dating back to the work of Gold (1948), SOAEs occur when the cellular control mechanisms needed to hold a hair cell close to the critical point break down:

> ''Because self-tuning positions the system slightly on the oscillating side of the critical point, self-tuned criticality provides a natural explanation for [spontaneous] otoacoustic emissions. In its normal working state, the inner ear would generate faint sounds with a broad range of frequencies. If the feedback mechanism were to fail in certain cells, the spontaneous oscillations could become large enough for distinct tones to be emitted.'' (Camalet *et al.*, 2000).

In this guise, the local-oscillator model has been repeatedly invoked to argue that outer-hair-cell (OHC) somatic motility is unlikely to constitute the ''active process'' in mammalian hearing. Martin and Hudspeth (1999, 2001; Martin *et al.*, 2003), for example, question the role of OHC somatic motility in the generation of mammalian SOAEs (see also Köppl, 1995; Martin *et al.*, 2001; Duke, 2002; Jülicher *et al.*, 2003). They note that although spontaneous movements have been reported in nonmammalian hair bundles ''there have been no observations of spontaneous outer-hair-cell contractions.'' Since they claim that ''unprovoked mechanical oscillations of some constituent of the inner ear *must* underlie the production of spontaneous otoacoustic emissions'' (Martin *et al.*, 2003, emphasis added), the evident conclusion is that mammalian SOAEs—and, by implication, the mammalian cochlear amplifier—require active hair-bundle motility.[23]

But Martin and Hudspeth's argument rests on a logical fallacy: that what's true of the whole must be true of the parts (the fallacy of division); that because the ear oscillates spontaneously some of its cellular constituents must do so themselves, and, furthermore, that only the autonomous oscillation of the ear's constituent parts can explain the spontaneous emission of sound by the whole.

We argue here, however, that most mammalian SOAEs arise not through autonomous cellular oscillations but through the collective action of the entire cochlea. SOAEs are not primarily the result of ''unprovoked movements'' of cellular constituents of the cochlear amplifier; rather, they are continually self-evoking stimulus–frequency OAEs that arise via the multiple internal reflection and coherent amplification of traveling-wave energy within the cochlea. As Kemp and others long ago suggested, the ''bifurcation'' responsible for the creation of self-sustaining SOAEs can arise *globally* rather than locally, much like that in a laser oscillator (e.g., Kemp, 1979a, b; Talmadge and Tubis, 1993; Zweig and Shera, 1995).

The global standing-wave model thus reverses the chain of causality inherent in the local-oscillator model: the mammalian ear does not whistle because individual hair cells oscillate spontaneously; rather, hair cells oscillate spontaneously because the ear whistles. Not only is the whole ''more than the sum of its parts,'' but the parts acquire new proper-

ties by virtue of their embedding in the whole. The apparent absence of spontaneous contractions in isolated OHCs has been presented as *primae facie* evidence against a role for somatic motility as the primary motor element underlying the mammalian cochlear amplifier (e.g., Martin and Hudspeth, 1999, 2001; Martin *et al.*, 2001, 2003; Jülicher *et al.*, 2003). Although a strong reductionist bias in our thinking may render these arguments superficially compelling, the logic that supports them is evidently fallacious.

Many qualitative emission phenomena, including the spontaneous production of sound, are no doubt generic to mechanical systems (such as the inner ears of frogs, lizards, birds, and mammals) that contain coupled arrays of active, nonlinear oscillators tuned to different frequencies. Although the existence and qualitative features of SOAEs may be generic, their quantitative properties (e.g., their bandwidths, their frequency separations, their interactions with one another and with external tones, their relationship to other emission types) presumably depend on details of the morphology, the physiology, and the hydrodynamics of the systems that produce them. Indeed, quantitative differences in features such as these do distinguish mammalian and nonmammalian SOAEs (e.g., van Dijk and Wit, 1990a; Köppl, 1995; van Dijk *et al.*, 1998), and to some extent even the SOAEs from different mammals (e.g., Ohyama *et al.*, 1991; Long *et al.*, 2000). Just as one can construct functional lasers around a variety of gain media, so one expects to find qualitative family resemblances among SOAEs arising from hearing organs that employ diverse strategies for enhancing their frequency selectivity and sensitivity to sound (e.g., Martin and Hudspeth, 1999; Liberman *et al.*, 2002); much more surprising indeed would be the finding that a single quantitative theory provides a satisfactory explanation for them all.

ACKNOWLEDGMENTS

The author gratefully acknowledges stimulating discussions with and/or helpful comments on the manuscript from John J. Guinan, Jont B. Allen, Pim van Dijk, Paul F. Fahey, K. Domenica Karavitaki, Geoffrey A. Manley, Stephen T. Neely, Sunil Puria, Carrick L. Talmadge, Arnold Tubis, Robert H. Withnell, and an anonymous reviewer. This work was supported by Grant No. R01 DC03687 from the NIDCD, National Institutes of Health.

[1]Previewing answers to these questions provided by the global standing-wave model, we note that the model predictions hinge on the ''standing-wave quantization condition,'' which determines the set of possible SOAE frequencies via Eq. (5) and characteristic SOAE spacings via Eq. (11). According to the theory of coherent-reflection filtering, the modal value of the characteristic SOAE spacing can be traced to the value of the wavelength of the traveling wave at its peak (or, equivalently, to the group delay at the peak of the basilar-membrane transfer function).

[2]For example, the cochlear reflectance $R(f)$ can be written as the product of R_x with the forward ($T^+_{0\to x}$) and reverse ($T^-_{x\to 0}$) traveling-wave transfer functions (e.g., $R=T^+_{0\to x}R_xT^-_{x\to 0}$) only in the unrealistic case that wave reflection/re-emission at frequency f occurs at the single point x.

[3]The stimulus source pressure $P_0(f)$ is the ear-canal pressure that would be measured if R were zero. In practice it is usually obtained by calibrating the stimulus earphone at moderate to high sound intensities (i.e., by rescaling the earphone pressure measured when $|P_{\mathrm{SFOAE}}/P_0|\ll 1$).

[4]G_{mert} is the product, $T^+_{\mathrm{me}}T^-_{\mathrm{me}}$, of the forward and reverse middle-ear pressure transfer functions measured at sound intensities where $|P_{\mathrm{SFOAE}}/P_0|\ll 1$. The forward pressure transfer function is defined by $T^+_{\mathrm{me}}\equiv(P_{\mathrm{v}}-P_{\mathrm{t}})/P_{\mathrm{ec}}$, where P_{v} and P_{t} are, respectively, the pressures in the scala vestibuli and scala tympani at the base of the cochlea; P_{ec} is the pressure in the ear canal. The middle ear is presumed driven in the ''forward'' direction with a sound source in the ear canal. Similarly, the reverse pressure transfer function is defined by $T^-_{\mathrm{me}}\equiv P_{\mathrm{ec}}/(P_{\mathrm{v}}-P_{\mathrm{t}})$, where the middle ear is now presumed driven from within the cochlea. Note that T^-_{me} depends on the characteristics of the transducer assembly used to measure P_{ec}; Eq. (2) assumes that this same transducer is used during the measurement of P_{SFOAE}. Since $|P_{\mathrm{t}}/P_{\mathrm{v}}|\ll 1$ (Nedzelnitsky, 1980), T^+_{me} and T^-_{me} can be approximated by measurements made in the scala vestibuli (e.g., $T^+_{\mathrm{me}}\approx P_{\mathrm{v}}/P_{\mathrm{ec}}$).

[5]Equation (2) assumes that the cochlear input impedance at frequency f is approximately real at intensities such that $|P_{\mathrm{SFOAE}}/P_0|\ll 1$ (e.g., Aibara *et al.*, 2001). Reality of the cochlear input impedance is guaranteed by the tapering symmetry manifest, for example, by the cochlea of the cat (Shera and Zweig, 1991b). Shera and Zweig (1991a) discuss the more general case in which the cochlear input impedance is complex and the characteristic wave impedances of the cochlear transmission line depend on the direction of propagation.

[6]The reflection coefficient R_{stapes} has the value $R_{\mathrm{stapes}}=r^-+[t^+t^-R_{\mathrm{s}}/(1-r^+R_{\mathrm{s}})]$, where the functions $r^\pm$ and $t^\pm$ are the reflectance and transmittance coefficients characterizing the residual ear-canal space and middle-ear (Shera and Zweig, 1992a) and R_{s} is the Thévenin-equivalent reflectance of the ear-canal acoustic load. Talmadge *et al.* (1998) derive formulas for R_{stapes} and G_{mert} valid for specific models for the middle-ear, ear-canal space, and earphone.

[7]The equation $RR_{\mathrm{stapes}}=1$ thus defines the ''instability modes'' of this linear analysis (Talmadge and Tubis, 1993; Talmadge *et al.*, 1998). Note that because little energy escapes from the cochlea as $|R_{\mathrm{staples}}|\to 1$, the boundary conditions optimal for producing large intracochlear standing waves are simultaneously those making their detection in the ear canal most difficult.

[8]In the active model, standing-wave amplitudes are actively maintained by wave amplification; in the passive model, they are driven by ongoing biological noise.

[9]Kemp's (1979b) original standing-wave model uses an approximate form of the quantization condition valid over frequency intervals roughly corresponding to $|\Delta n|\lesssim 2$. Kemp's condition can be obtained from Eq. (5) by approximating $\angle R(f)$ by $-\omega T(f)$, where $T(f)$ is the emission group delay at the stapes, defined by $T(f)=-d\angle R/d\omega$, with $\omega=2\pi f$. Kemp's formula would be equivalent to Eq. (5) if $T(f)$ were independent of f; in fact, however, $T(f)\sim 1/f^{1-\alpha}$ with $\alpha\approx 0.37$ (see Table I and Shera and Guinan, 2003). Kemp's formula applies over frequency intervals sufficiently small that $T(f)$ can be regarded as constant. An estimate, Δf_{K}, of the size of this interval follows from the requirement that $|d\ln T/df|\Delta f_{\mathrm{K}}<\epsilon$, where $\epsilon\ll 1$. Evaluating the logarithmic derivative and expressing Δf_{K} in terms of the characteristic spacing $\overline{\Delta f}_{\mathrm{SOAE}}$ yields $\Delta f_{\mathrm{K}}<\epsilon[\bar{N}_{\mathrm{SOAE}}/(1-\alpha)]\overline{\Delta f}_{\mathrm{SOAE}}$, where $\bar{N}_{\mathrm{SOAE}}$ is the modal value of N_{SOAE}. Taking $\epsilon\sim 0.15$ and $\bar{N}_{\mathrm{SOAE}}\approx 15$ at 1500 Hz yields $\Delta f_{\mathrm{K}}/\overline{\Delta f}_{\mathrm{SOAE}}\lesssim 4$, or, equivalently, $|\Delta n|\lesssim 2$.

[10]SOAEs with frequencies within 2 Hz of the value $2f_1-f_2$ computed by using other SOAE pairs in the same ear as primaries f_1 and f_2 were tagged as likely to represent lower-sideband cubic distortion products formed by the interaction of other, independent SOAEs in the same ear (cf. Burns *et al.*, 1984; Talmadge *et al.*, 1993). SOAE pairs that included one or more of these probable ''distortion-product SOAEs'' (16 of the 503 pairs of adult emissions) were excluded both from Fig. 3 and from the power-law fit.

[11]Comparisons of psychoacoustic and emission cancellation levels for $(2f_1-f_2)$-combination-tones (Zwicker and Harris, 1990) suggest that a 0-dB SPL SOAE may produce as much intracochlear excitation as a 35–50-dB SPL tone presented in the ear canal. Interpretation of these measurements, however, is complicated by a number of factors, including uncontrolled mixing of reflection- and distortion-source DPOAE components (e.g., Kalluri and Shera, 2001) and uncertainties associated with the psychoacoustic cancellation paradigm (e.g., Smoorenburg, 1974; Siegel and Borneman, 1999).

[12]According to the measurements and analysis of Neely *et al.* (1988), evoked OAE latencies measured at sound level $L+\Delta L$ (in dB SPL) will

differ from those measured at level L by a frequency-independent factor of approximately $c^{-\Delta L/100}$, with $c=5$. This value is likely to be an upper bound; Neely *et al.*'s characterization presumably overestimates the intensity dependence of OAE latencies at low sound levels, where cochlear mechanics becomes approximately linear.

[13]R_{stapes} has the form $R_{\text{stapes}}=(Z_{\text{mer}}-Z_{\text{c}})/(Z_{\text{mer}}+Z_{\text{c}})$, where Z_{c} is the cochlear input impedance (assumed resistive) and Z_{mer} is the ''reverse middle-ear impedance'' (Puria, 2003).

[14]With the subject reclining comfortably in a sound-isolated chamber, ear-canal pressure was transduced using an Etymotic Research ER-10c microphone and digitized at a sampling rate of 12.2 kHz using a Tucker-Davis System III running custom software. Eighty seconds of data were filtered using a tenth-order, recursive-exponential bandpass filter (Shera and Zweig, 1993a; Kalluri and Shera, 2001) centered on the nominal SOAE frequency ($f_{\text{SOAE}}=2449.6$ Hz). The filter bandwidth (approximately 200 Hz) was taken to be much larger than the emission bandwidth (approximately 1 Hz). The analytic signal, $z_{\text{SOAE}}(t)$, of the filtered waveform was then obtained using the Hilbert transform (e.g., Cohen, 1995) and the function $\tilde{p}_{\text{SOAE}}(t)$ computed using the equation $\tilde{p}_{\text{SOAE}}(t)=z_{\text{SOAE}}(t)e^{-2\pi i f_{\text{SOAE}}t}$. Multiplication by the phasor $e^{-2\pi i f_{\text{SOAE}}t}$ isolates the slowly varying components of $z_{\text{SOAE}}(t)$ by dividing out the rapid phase rotation due to the carrier (SOAE) frequency. Temporal resolution was improved by a factor of 4 using bandlimited $\sin(x)/x$ interpolation prior to computing the probability distribution $\mathcal{D}[\tilde{p}_{\text{SOAE}}(t)]$.

[15]Many of these dynamic features are best illustrated by animating the time evolution of $\mathcal{D}[\tilde{p}(t)]$ (see http://epl.meei.harvard.edu/~shera/soae-movie.zip). To keep the animation short (and continually interesting) the time interval between movie frames was increased as the square of the elapsed time. The statistical power of the distribution therefore increases linearly from frame to frame.

[16]The Bialek–Wit analysis actually involves computing the distribution $\mathcal{D}[p_{\text{SOAE}}(t)]=\mathcal{D}[\text{Re}\{z_{\text{SOAE}}(t)\}]=\mathcal{D}[\text{Re}\{\tilde{p}_{\text{SOAE}}(t)e^{2\pi i f_{\text{SOAE}}t}\}]$ (see footnote 14 for an explanation of the notation). Because it includes smearing effects due to rapid phase rotation at the carrier frequency (f_{SOAE}), the Bialek–Wit distribution is generally much smoother than $\mathcal{D}[\text{Re}\{\tilde{p}_{\text{SOAE}}(t)\}]$. The two distributions are nearly identical, however, when computed over time intervals long compared to the reciprocal of the emission bandwidth.

[17]For example, an autonomous cellular oscillator would not experience strong, bidirectional coupling to the external environment if the stapes and adjoining structures somehow conspired to present a nearly reflectionless boundary. Although normal, in vivo values of R_{stapes} remain uncertain, typical transducer assemblies have Thévenin-equivalent reflectances close to 1 in magnitude; the condition $|R_{\text{stapes}}|\ll 1$ therefore seems unlikely to apply in most experimental situations.

[18]Incoherent reflection from large punctate perturbations may, however, dominate in certain pathologies or in specialized cochleae, such as in the ''auditory fovea'' of the CF-FM bat (e.g., Kössl and Vater, 1995), in which the mechanical properties of the cochlear partition change rapidly with position.

[19]Local scaling symmetry implies that N_{BM} also equals the group delay of the basilar-membrane transfer function at its peak, measured in periods of the CF (Shera and Guinan, 2003).

[20]Kemp's (1979b) original standing-wave model was published before the term ''cochlear amplifier'' had even been coined (Neely, 1983; Davis, 1983).

[21]A similar problem is encountered when trying to determine whether the middle-ear reflectance has magnitude greater than 1 at frequencies near SOAEs (e.g., Allen *et al.*, 1995; Tubis and Talmadge, 1998; Burns *et al.*, 1998).

[22]For a critique of this claim, see Zweig (2003), and the comments and discussion reprinted following the text.

[23]Even when a possible amplificatory function of OHC somatic motility is acknowledged, SOAEs are invariably presumed to arise via autonomous subcellular oscillations, with the hair bundle retaining its role as putative causal agent (e.g., Duke, 2002): ''In the mammalian cochlea, the outer hair cells are widely believed to power the movement of the basilar membrance. It remains unclear, however, whether the outer-hair-cell motor is itself a Hopf oscillator, or whether it is simply an additional linear amplifier that boosts oscillations generated by the hair bundle. Spontaneous oscillations of an outer hair cell have never been observed.'' Jülicher *et al.* (2003) argue along similar lines: ''The concept of self-tuned critical oscillations applies essentially to all vertebrate ears since they all have spontaneous otoacoustic emissions. However, the question of what are the underlying specific mechanisms at the origin of spontaneous oscillations is a subject of active research. In mammals, it is widely thought that outer hair cells are the active elements and thus might contain mechanical oscillators. However, even though it is well established that outer hair cells can contract their cell bodies in the presence of electrical stimuli, no spontaneous oscillations have so far been observed.''

Aibara, R., Welsh, J. T., Puria, S., and Goode, R. L. (**2001**). ''Human middle-ear sound transfer function and cochlear input impedance,'' Hear. Res. **152**, 100–109.

Allen, J. B., and Fahey, P. F. (**1992**). ''Using acoustic distortion products to measure the cochlear amplifier gain on the basilar membrane,'' J. Acoust. Soc. Am. **92**, 178–188.

Allen, J. B., Shaw, G., and Kimberley, B. P. (**1995**). ''Characterization of the nonlinear ear canal impedance at low sound levels,'' Assoc. Res. Otolaryngol. Abs. **18**, 797.

Allen, J. B. (**2001**). ''Nonlinear cochlear signal processing,'' in *Physiology of the Ear*, edited by A. F. Jahn and J. Santos-Sacchi (Singular, San Diego), pp. 393–442.

Avan, P., Büki, B., Maat, B., Dordain, M., and Wit, H. P. (**2000**). ''Middle-ear influence on otoacoustic emissions. I. Noninvasive investigation of the human transmission apparatus and comparison with model results,'' Hear. Res. **140**, 189–201.

Bell, A. (**1992**). ''Circadian and menstrual rhythms in frequency variations of spontaneous otoacoustic emissions from human ears,'' Hear. Res. **58**, 91–100.

Bialek, W., and Wit, H. P. (**1984**). ''Quantum limits to oscillator stability: Theory and experiments on acoustic emissions from the human ear,'' Phys. Lett. **104A**, 173–178.

Braun, M. (**1997**). ''Frequency spacing of multiple spontaneous otoacoustic emissions shows relation to critical bands: A large-scale cumulative study,'' Hear. Res. **114**, 197–203.

Bredberg, G. (**1968**). ''Cellular patterns and nerve supply of the human organ of Corti,'' Acta Oto-Laryngol., Suppl. **236**, 1–135.

Büki, B., Chomicki, A., Dordain, M., Lemaire, J., Wit, H. P., Chazal, J., and Avan, P. (**2000**). ''Middle-ear influence on otoacoustic emissions. II. Contributions of posture and intracranial pressure,'' Hear. Res. **140**, 202–211.

Burns, E. M., Arehart, K. H., and Campbell, S. L. (**1992**). ''Prevalence of spontaneous otoacoustic emissions in neonates,'' J. Acoust. Soc. Am. **91**, 1571–1575.

Burns, E. M., Harrison, W. A., Bulen, J. C., and Keefe, D. H. (**1993**). ''Voluntary contraction of middle ear muscles: Effects on input impedance, energy reflectance and spontaneous otoacoustic emissions,'' Hear. Res. **67**, 117–127.

Burns, E. M., Keefe, D. H., and Ling, R. (**1998**). ''Energy reflectance in the ear canal can exceed unity near spontaneous otoacoustic emission frequencies,'' J. Acoust. Soc. Am. **103**, 462–474.

Burns, E. M., Strickland, E. A., Tubis, A., and Jones, K. (**1984**). ''Interactions among spontaneous otoacoustic emissions. I. Distortion products and linked emissions,'' Hear. Res. **16**, 271–278.

Camalet, S., Duke, T., Jülicher, F., and Prost, J. (**2000**). ''Auditory sensitivity provided by self-tuned critical oscillations of hair cells,'' Proc. Natl. Acad. Sci. U.S.A. **97**, 3183–3188.

Cleveland, W. S. (**1993**). *Visualizing Data* (Hobart, Summit, NJ).

Cohen, L. (**1995**). *Time-Frequency Analysis* (Prentice Hall PTR, Upper Saddle River, NJ).

Crawford, A. C., and Fettiplace, R. (**1985**). ''The mechanical properties of ciliary bundles of turtle cochlear hair cells,'' J. Physiol. (London) **364**, 359–379.

Dallmayr, C. (**1985**). ''Spontane oto-akustiche Emissionen, Statistik und Reaktion auf akustiche Störtöne,'' Acustica **59**, 67–75.

Davis, H. (**1983**). ''An active process in cochlear mechanics,'' Hear. Res. **9**, 79–90.

Denk, W., and Webb, W. W. (**1992**). ''Forward and reverse transduction at the limit of sensitivity studied by correlating electrical and mechanical fluctuations in frog saccular hair cells,'' Hear. Res. **60**, 89–102.

de Kleine, E., Wit, H. P., van Dijk, P., and Avan, P. (**2000**). ''The behavior of spontaneous otoacoustic emissions during and after postural changes,'' J. Acoust. Soc. Am. **107**, 3308–3316.

Dhar, S., Talmadge, C. L., Long, G. R., and Tubis, A. (**2002**). ''Multiple internal reflections in the cochlea and their effect on DPOAE fine structure,'' J. Acoust. Soc. Am. **112**, 2882–2897.

Duke, T. (**2002**). ''The power of hearing,'' Phys. World **15**, 29–33.

Egolf, D. P., Kennedy, W. A., and Larson, V. D. (**1992**). ''Occluded-ear simulator with variable acoustic properties,'' J. Acoust. Soc. Am. **91**, 2813–2823.
Eguíluz, V. M., Ospeck, M., Choe, Y., Hudspeth, A. J., and Magnasco, M. O. (**2000**). ''Essential nonlinearities in hearing,'' Phys. Rev. Lett. **84**, 5232–5235.
Engström, H., Ades, H. W., and Andersson, A. (**1966**). *Structural Pattern of the Organ of Corti* (Williams and Wilkins, Baltimore).
Geisler, C. D. (**1998**). *From Sound to Synapse* (Oxford University Press, New York).
Gleich, O., and Narins, P. M. (**1988**). ''The phase response of primary auditory afferents in a songbird (*Sturnus vulgaris L.*),'' Hear. Res. **32**, 81–91.
Golay, M. J. E. (**1961**). ''Note on coherence vs narrow-bandedness in regenerative oscillators, masers, lasers, etc.,'' Proc. IRE **49**, 958–959.
Gold, T. (**1948**). ''Hearing. II. The physical basis of the action of the cochlea,'' Proc. R. Soc. London, Ser. B **135**, 492–498.
Greenwood, D. D. (**1990**). ''A cochlear frequency-position function for several species—29 years later,'' J. Acoust. Soc. Am. **87**, 2592–2605.
Hauser, R., Probst, R., and Harris, F. P. (**1993**). ''Effects of atmospheric pressure variation on spontaneous, transiently evoked, and distortion product otoacoustic emissions in normal human ears,'' Hear. Res. **69**, 133–145.
Hillery, C. M., and Narins, P. M. (**1984**). ''Neurophysiological evidence for a traveling wave in the amphibian inner ear,'' Science (Washington, DC, U.S.) **225**, 1037–1039.
Hudspeth, A. J. (**1997**). ''Mechanical amplification of stimuli by hair cells,'' Curr. Opin. Neurobiol. **7**, 480–486.
Jülicher, F., Camalet, S., Prost, J., and Duke, T. A. J. (**2003**). ''Active amplification by critical oscillations,'' in *Biophysics of the Cochlea: From Molecules to Models*, edited by A. W. Gummer (World Scientific, Singapore), pp. 16–27.
Kalluri, R., and Shera, C. A. (**2001**). ''Distortion-product source unmixing: A test of the two-mechanism model for DPOAE generation,'' J. Acoust. Soc. Am. **109**, 622–637.
Keefe, D. H., Bulen, J. C., Arehart, K. H., and Burns, E. M. (**1993**). ''Ear-canal impedance and reflectance coefficient in human infants and adults,'' J. Acoust. Soc. Am. **94**, 2617–2638.
Kemp, D. T., and Chum, R. A. (**1980**). ''Observations on the generator mechanism of stimulus frequency acoustic emissions—Two tone suppression,'' in *Psychophysical Physiological and Behavioural Studies in Hearing*, edited by G. V. D. Brink and F. A. Bilsen (Delft University Press, Delft), pp. 34–42.
Kemp, D. T. (**1979a**). ''Evidence of mechanical nonlinearity and frequency selective wave amplification in the cochlea,'' Arch. Oto-Rhino-Laryngol. **224**, 37–45.
Kemp, D. T. (**1979b**). ''The evoked cochlear mechanical response and the auditory microstructure—Evidence for a new element in cochlear mechanics,'' Scand. Audiol. Suppl. **9**, 35–47.
Kemp, D. T. (**1981**). ''Physiologically active cochlear micromechanics—one source of tinnitus,'' in *Tinnitus*, edited by D. Evered and G. Lawrenson (Pitman, London), pp. 54–81.
Kemp, D. T. (**2002**). ''Exploring cochlear status with otoacoustic emissions: The potential for new clinical applications,'' in *Otoacoustic Emissions: Clinical Applications*, 2nd ed., edited by M. S. Robinette and T. J. Glattke (Thieme, New York), pp. 1–47.
Konrad-Martin, D., Neely, S. T., Keefe, D. H., Dorn, P. A., and Gorga, M. P. (**2001**). ''Sources of distortion product otoacoustic emissions revealed by suppression experiments and inverse fast Fourier transforms in normal ears,'' J. Acoust. Soc. Am. **109**, 2862–2869.
Köppl, C. (**1995**). ''Otoacoustic emissions as an indicator for active cochlear mechanics: A primitive property of vertebrate auditory organs,'' in *Advances in Hearing Research*, edited by G. A. Manley, G. M. Klump, C. Köppl, H. Fastl, and H. Oeckinghaus (World Scientific, Singapore), pp. 207–218.
Kössl, M. and Vater, M. (**1995**). ''Cochlear structure and function in bats,'' in *Hearing by Bats*, edited by A. N. Popper and R. R. Fay (Springer, New York), pp. 191–234.
Liberman, M. C., Gao, J., He, D. Z. Z., Wu, X., Jia, S., and Zuo, J. (**2002**). ''Prestin is required for electromotility of the outer hair cell and for the cochlear amplifier,'' Nature (London) **419**, 300–304.
Long, G. R., Schaffer, L. A., Dhar, S., and Talmadge, C. L. (**2000**). ''Cross species comparison of otoacoustic fine-structure,'' in *Recent Developments in Auditory Mechanics*, edited by H. Wada, T. Takasaka, K. Ikeda, K. Ohyama, and T. Koike (World Scientific, Singapore), pp. 367–373.
Lonsbury-Martin, B. L., Martin, G. K., Probst, R., and Coats, A. C. (**1988**). ''Spontaneous otoacoustic emissions in the nonhuman primate. II. Cochlear anatomy,'' Hear. Res. **33**, 69–94.
Lonsbury-Martin, B. L., and Martin, G. K. (**2001**). ''Otoacoustic emissions,'' in *Physiology of the Ear*, edited by A. F. Jahn and J. Santos-Sacchi (Singular, San Diego), pp. 443–480.
Manley, G. A., Yates, G. K., and Köppl, C. (**1990**). ''Peripheral auditory processing in the bobtail lizard Tiliqua rugosa: IV. Phase locking of auditory-nerve fibers,'' J. Comp. Physiol., A **167**, 129–138.
Manley, G. A. (**1990**). *Peripheral Hearing Mechanisms in Reptiles and Birds* (Springer, Berlin).
Manley, G. A. (**2001**). ''Evidence for an active process and a cochlear amplifier in nonmammals,'' J. Neurophysiol. **86**, 541–549.
Martin, P., Hudspeth, A. J., and Jülicher, F. (**2001**). ''Comparison of a hair bundle's spontaneous oscillations with its response to mechanical stimulation reveals the underlying active process,'' Proc. Natl. Acad. Sci. U.S.A. **98**, 14380–14385.
Martin, P., and Hudspeth, A. J. (**1999**). ''Active hair-bundle movements can amplify a hair cell's response to oscillatory mechanical stimuli,'' Proc. Natl. Acad. Sci. U.S.A. **96**, 14306–14311.
Martin, P., and Hudspeth, A. J. (**2001**). ''Compressive nonlinearity in the hair bundles active response to mechanical stimulation,'' Proc. Natl. Acad. Sci. U.S.A. **98**, 14386–14391.
Martin, P., Jülicher, F., and Hudspeth, A. J. (**2003**). ''The contribution of transduction channels and adaptation motors to the hair cell's active process,'' in *Biophysics of the Cochlea: From Molecules to Models*, edited by A. W. Gummer (World Scientific, Singapore), pp. 3–15.
Murphy, W. J., Talmadge, C. L., Tubis, A., and Long, G. R. (**1995a**). ''Relaxation dynamics of spontaneous otoacoustic emissions perturbed by external tones. I. Response to pulsed single-tone suppressors,'' J. Acoust. Soc. Am. **97**, 3702–3710.
Murphy, W. J., Tubis, A., Talmadge, C. L., and Long, G. R. (**1995b**). ''Relaxation dynamics of spontaneous otoacoustic emissions perturbed by external tones. II. Suppression of interacting emissions,'' J. Acoust. Soc. Am. **97**, 3711–3720.
Murphy, W. J., Tubis, A., Talmadge, C. L., Long, G. R., and Krieg, E. F. (**1996**). ''Relaxation dynamics of spontaneous otoacoustic emissions perturbed by external tones. III. Response to a single tone at multiple suppression levels,'' J. Acoust. Soc. Am. **100**, 3979–3982.
Nedzelnitsky, V. (**1980**). ''Sound pressures in the basal turn of the cat cochlea,'' J. Acoust. Soc. Am. **68**, 1676–1689.
Neely, S. T., Norton, S. J., Gorga, M. P., and Jesteadt, W. (**1988**). ''Latency of auditory brain-stem responses and otoacoustic emissions using tone-burst stimuli,'' J. Acoust. Soc. Am. **83**, 652–656.
Neely, S. T. (**1983**). ''The cochlear amplifier,'' in *Mechanics of Hearing*, edited by E. Boer and M. A. Viergever (Martinus Nijhoff, The Hague), pp. 111–118.
Norton, S. J., and Neely, S. T. (**1987**). ''Tone-burst-evoked otoacoustic emissions from normal-hearing subjects,'' J. Acoust. Soc. Am. **81**, 1860–1872.
Ohyama, K., Wada, H., Kobayashi, T., and Takasaka, T. (**1991**). ''Spontaneous otoacoustic emissions in the guinea pig,'' Hear. Res. **56**, 111–121.
Oxenham, A. J., and Shera, C. A. (**2003**). ''Estimates of human cochlear tuning at low levels using forward and simultaneous masking,'' J. Assoc. Res. Otolaryngol. (in press).
Pang, X. D., and Peake, W. T. (**1986**). ''How do contractions of the stapedius muscle alter the acoustic properties of the ear?,'' in *Peripheral Auditory Mechanisms*, edited by J. B. Allen, J. L. Hall, A. Hubbard, S. T. Neely, and A. Tubis (Springer, Berlin), pp. 36–43.
Peake, W. T., and Ling, A., (**1980**). ''Basilar-membrane motion in the alligator lizard: Its relation to tonotopic organization and frequency selectivity,'' J. Acoust. Soc. Am. **67**, 1736–1745.
Peake, W. T., Rosowski, J. J., and Lynch, T. J. (**1992**). ''Middle-ear transmission: Acoustic versus ossicular coupling in cat and human,'' Hear. Res. **57**, 245–268.
Puria, S., Peake, W. T., and Rosowski, J. J. (**1997**). ''Sound-pressure measurements in the cochlear vestibule of human-cadaver ears,'' J. Acoust. Soc. Am. **101**, 2754–2770.
Puria, S. (**2003**). ''Measurements of human middle ear forward and reverse acoustics: Implications for otoacoustic emissions,'' J. Acoust. Soc. Am. **113**, 2773–2789.
Rice, S. O. (**1954**). ''Mathematical analysis of random noise,'' in *Selected Papers on Noise and Stochastic Processes*, edited by N. Wax (Dover, New York), pp. 133–294.
Russell, A. F. (**1992**). ''Heritability of spontaneous otoacoustic emissions,'' Ph.D. thesis, University of Illinois.

Russell, I. J., and Kössl, M. (**1999**). ''Micromechanical responses to tones in the auditory fovea of the greater mustached bat's cochlea,'' J. Neurophysiol. **82**, 676–686.
Schloth, E., and Zwicker, E. (**1983**). ''Mechanical and acoustical influences on spontaneous otoacoustic emissions,'' Hear. Res. **11**, 285–293.
Schloth, E. (**1983**). ''Relation between spectral composition of spontaneous otoacoustic emissions and fine-structure of threshold in quiet,'' Acustica **53**, 250–256.
Shera, C. A., and Guinan, J. J. (**1999**). ''Evoked otoacoustic emissions arise by two fundamentally different mechanisms: A taxonomy for mammalian OAEs,'' J. Acoust. Soc. Am. **105**, 782–798.
Shera, C. A., Guinan, J. J., and Oxenham, A. J. (**2002**). ''Revised estimates of human cochlear tuning from otoacoustic and behavioral measurements,'' Proc. Natl. Acad. Sci. U.S.A. **99**, 3318–2232.
Shera, C. A., and Guinan, J. J. (**2003**). ''Stimulus-frequency-emission group delay: A test of coherent reflection filtering and a window on cochlear tuning,'' J. Acoust. Soc. Am. **113**, 2762–2772.
Shera, C. A., and Zweig, G. (**1991a**). ''Reflection of retrograde waves within the cochlea and at the stapes,'' J. Acoust. Soc. Am. **89**, 1290–1305.
Shera, C. A., and Zweig, G. (**1991b**). ''A symmetry suppresses the cochlear catastrophe,'' J. Acoust. Soc. Am. **89**, 1276–1289.
Shera, C. A., and Zweig, G. (**1992a**). ''Analyzing reverse middle-ear transmission: Noninvasive Gedankenexperiments,'' J. Acoust. Soc. Am. **92**, 1371–1381.
Shera, C. A., and Zweig, G. (**1992b**). ''Middle-ear phenomenology: The view from the three windows,'' J. Acoust. Soc. Am. **92**, 1356–1370.
Shera, C. A., and Zweig, G. (**1993a**). ''Noninvasive measurement of the cochlear traveling-wave ratio,'' J. Acoust. Soc. Am. **93**, 3333–3352.
Shera, C. A., and Zweig, G. (**1993b**). ''Order from chaos: Resolving the paradox of periodicity in evoked otoacoustic emission,'' in *Biophysics of Hair Cell Sensory Systems*, edited by H. Duifhuis, J. W. Horst, P. van Dijk, and S. M. van Netten (World Scientific, Singapore), pp. 54–63.
Siegel, J. H., and Borneman, A. L. (**1999**). ''Comparable measures of perceptual combination tones and distortion-product otoacoustic emissions,'' Assoc. Res. Otolaryngol. Abs. **22**, 393.
Siegman, A. E. (**1986**). *Lasers* (University Science, Sausalito, CA).
Sisto, R., and Moleti, A. (**1999**). ''Modeling otoacoustic emissions by active nonlinear oscillators,'' J. Acoust. Soc. Am. **106**, 1893–1906.
Smolders, J. W. T., and Klinke, R. (**1986**). ''Synchronized responses of primary auditory fiber populations in *Caiman crocodilus* (*L*.) to single tones and clicks,'' Hear. Res. **24**, 89–103.
Smoorenburg, G. F. (**1974**). ''On the mechanisms of combination tone generation and lateral inhibition in hearing,'' in *Facts and Models in Hearing*, edited by E. Zwicker and E. Terhardt (Springer, Berlin), pp. 332–342.
Talmadge, C. L., Long, G. R., Murphy, W. J., and Tubis, A. (**1993**). ''New off-line method for detecting spontaneous otoacoustic emission in human subjects,'' Hear. Res. **71**, 170–182.
Talmadge, C. L., Tubis, A., Long, G. R., and Piskorski, P. (**1998**). ''Modeling otoacoustic emission and hearing threshold fine structures,'' J. Acoust. Soc. Am. **104**, 1517–1543.
Talmadge, C. L., Tubis, A., Wit, H. P., and Long, G. R. (**1991**). ''Are spontaneous otoacoustic emissions generated by self-sustained cochlear oscillators?,'' J. Acoust. Soc. Am. **89**, 2391–2399.
Talmadge, C. L., and Tubis, A. (**1993**). ''On modeling the connection between spontaneous and evoked otoacoustic emissions,'' in *Biophysics of Hair Cell Sensory Systems*, edited by H. Duifhuis, J. W. Horst, P. van Dijk, and S. M. van Netten (World Scientific, Singapore), pp. 25–32.
Tubis, A., and Talmadge, C. L. (**1998**). ''Ear canal reflectance in the presence of spontaneous otoacoustic emissions. I. Limit-cycle oscillator model,'' J. Acoust. Soc. Am. **103**, 454–461.
Voss, S. E., and Allen, J. B. (**1994**). ''Measurement of acoustic impedance and reflectance in the human ear canal,'' J. Acoust. Soc. Am. **95**, 372–384.
van Dijk, P., Manley, G. A., Gallo, L., Pavusa, A., and Taschenberger, G. (**1996**). ''Statistical properties of spontaneous otoacoustic emissions in one bird and three lizard species,'' J. Acoust. Soc. Am. **100**, 2220–2227.
van Dijk, P., Manley, G. A., and Gallo, L. (**1998**). ''Correlated amplitude fluctuations of spontaneous otoacoustic emissions in six lizard species,'' J. Acoust. Soc. Am. **104**, 1559–1564.
van Dijk, P., and Wit, H. P. (**1990a**). ''Amplitude and frequency fluctuations of spontaneous otoacoustic emissions,'' J. Acoust. Soc. Am. **88**, 1779–1793.
van Dijk, P., and Wit, H. P. (**1990b**). ''Synchronization of spontaneous otoacoustic emissions to a $2f_1-f_2$ distortion product,'' J. Acoust. Soc. Am. **88**, 850–856.
van Hengel, P. W. J., Duifhuis, H., and van den Raadt, M. P. M. G. (**1996**). ''Spatial periodicity in the cochlea: The result of interaction of spontaneous emissions?,'' J. Acoust. Soc. Am. **99**, 3566–3571.
Wilson, J. P., and Sutton, G. J. (**1981**). ''Acoustic correlates of tonal tinnitus,'' in *Tinnitus*, edited by D. Evered and G. Lawrenson (Pitman, London), pp. 82–107.
Wilson, J. P. (**1980**). ''Evidence for a cochlear origin for acoustic re-emissions, threshold fine-structure, and tonal tinnitus,'' Hear. Res. **2**, 233–252.
Wright, A. A. (**1984**). ''Dimensions of the cochlear stereocilia in man and in guinea pig,'' Hear. Res. **13**, 89–98.
Zurek, P. M. (**1981**). ''Spontaneous narrow-band acoustic signals emitted by human ears,'' J. Acoust. Soc. Am. **69**, 514–523.
Zweig, G., and Shera, C. A. (**1995**). ''The origin of periodicity in the spectrum of evoked otoacoustic emissions,'' J. Acoust. Soc. Am. **98**, 2018–2047.
Zweig, G. (**1991**). ''Finding the impedance of the organ of Corti,'' J. Acoust. Soc. Am. **89**, 1229–1254.
Zweig, G. (**2003**). ''Cellular cooperation in cochlear mechanics,'' in *Biophysics of the Cochlea: From Molecules to Models*, edited by A. W. Gummer (World Scientific, Singapore), pp. 315–330.
Zwicker, E., and Harris, F. P. (**1990**). ''Psychoacoustical and ear canal cancellation of $(2f_1-f_2)$-distortion products,'' J. Acoust. Soc. Am. **87**, 2583–2591.
Zwicker, E., and Manley, G. (**1981**). ''Acoustical responses and suppression-period patterns in guinea pigs,'' Hear. Res. **4**, 43–52.
Zwicker, E., and Peisl, W. (**1990**). ''Cochlear preprocessing in analog models, in digital models, and in human inner ear,'' Hear. Res. **44**, 209–216.
Zwicker, E., and Schloth, E. (**1984**). ''Interrelation of different otoacoustic emissions,'' J. Acoust. Soc. Am. **75**, 1148–1154.
Zwicker, E. (**1988**). ''The inner ear, a sound processing and a sound emitting system,'' J. Acoust. Soc. Jpn. **9**, 59–74.
Zwicker, E. (**1989**). ''Otoacoustic emissions and cochlear travelling waves,'' in *Cochlear Mechanisms—Structure, Function, and Models*, edited by J. P. Wilson and D. T. Kemp (Plenum, New York), pp. 359–366.